X-551-70-171
PREPRINT

NASA TM X- 65311

MINITRACK POSTDETECTION BANDWIDTH CONSIDERATIONS

T. J. GRENCHIK
C. W. MURRAY JR.

JUNE 1970

GODDARD SPACE FLIGHT CENTER
GREENBELT, MARYLAND

X-551-70-171

PREPRINT

MINITRACK POSTDETECTION BANDWIDTH CONSIDERATIONS

T. J. Grenchik

C. W. Murray, Jr.

JUNE 1970

Goddard Space Flight Center

Greenbelt, Maryland

MINITRACK POSTDETECTION BANDWIDTH CONSIDERATIONS

T. J. Grenchik

C. W. Murray, Jr.

ABSTRACT

A description of the Minitrack system and definition of the measurement made by the system is presented.

Design considerations relating to the phaselock loop response of the proposed postdetection filter are discussed. Under an assumed set of "worst case" orbital dynamics for the satellite (100 statute mile height circular orbit with a useful 10° overhead arc), a second order phaselock loop with a 10 Hz bandwidth is recommended for the filter.

The "gain" due to least squares smoothing of the Minitrack data at the output of the postdetection filter is calculated for a number of filter designs. For the 10 Hz equivalent double pole filter above, a sampling rate from 10 to 20 samples per second is recommended. It is shown that by increasing the rate above 20 samples per second the "gain" due to smoothing increases by approximately a db (decibel), while aggravating the data handling problem.

SUMMARY

The Minitrack system and its measurement are described and several potential error sources related to the system measurement are presented. The major source of error listed is the uncertainty in delay (fixed or time varying) in each of the antennas of the antenna pair prior to signal combining (or equivalently signal cross-correlation). From this major error source, a minimum of 10 arc seconds pointing error is postulated as the Minitrack system resolution.

A "worst case" orbit is assumed in order to establish rates of change of pointing angle which define the postdetection filter parameters. From a circular orbit of 100 statute miles height above the Minitrack station, there follows the requirement for a 10 Hz bandwidth, 2nd order phaselock loop filter design. Other parameters such as signal detection method and antenna gain remain fixed in this analysis. Signal to noise considerations then require adjustment of satellite effective radiated power.

The effect of least squares smoothing of the data at the output of the postdetection filter is investigated for a number of filter designs and bandwidths. Again a "worst case" orbit is assumed with the satellite passing directly overhead and the total arc of visibility taken as 10° (±5° from zenith). The "gain" in signal to noise ratio due to smoothing is defined and is seen to be a function of the satellite dynamics, the total time of visibility, the filter design and bandwidth. It is shown that the choice of a filter design cannot be based on the "gain" achieved

by smoothing. Once the design is fixed the least squares analysis aids in the selection of a sampling rate.

For the 10 Hz equivalent double pole filter recommended above, a sampling rate of 10 to 20 samples per second is recommended. This particular range of sampling rates will provide a sufficiently high "gain" while keeping the data handling at a minimum level.

CONTENTS

MINITRACK POSTDETECTION

BANDWIDTH CONSIDERATIONS

INTRODUCTION

The Minitrack system measures angles (direction cosines) to an orbiting spacecraft with reference to a ground station coordinate system by an interferometer technique. The system has been successfully used for tracking near-Earth satellites (reference 1) where angle rates are appreciable as compared to satellites at lunar distances and beyond.

This paper considers system design parameters for the postdetection filter of the Minitrack system and discusses the "gain" due to least squares smoothing of data at the output of the filter. The orbital dynamics and geometry which are assumed can be seen in Figure 1.

The satellite located at point S is in a circular orbit at an altitude h_s above the earth and is moving in a clockwise direction. The line of sight from the tracking station at point T to the satellite makes an angle θ (interferometer angle) with the local tangent. The central angle is α and the angle between line ST and SO is β. The system measurement is proportional to D cos θ where D is the length of the interferometer baseline.

From the changing geometry of Figure 1, design requirements are imposed upon the postdetection filter which define the filter shape and bandwidth. Selection of Minitrack system data rate follows this filter definition and it is shown that an optimum range of sampling rates exists that is practical with respect to Goddard/Minitrack Station data handling capabilities.

SYSTEM DESCRIPTION

Figure 2 shows a simplified block diagram of the Minitrack system. In this diagram a pair of antennas, separated by a baseline length, D, receives a signal $\sin \psi(t)$, where $\psi(t)$ is the time variant phase function of the incoming signal. The knowledgeable reader will immediately note that the ambiguity resolution system has not been included. This was done to simplify the description. For the reader without a Minitrack system background, References 2, 3, and 4 are recommended. The pair of fine antennas imparts a phase change $U[\theta(t)]$ and $V[\theta(t)]$ to the signal observed at the respective antennas. Because of the angle θ, the line-of-sight angle with respect to the local horizontal, a point on the wavefront, $\sin \psi(t)$, arrives at FINE ANTENNA "B" a time Δt later than at FINE ANTENNA "A". The difference in path length, Φ, is related to the line-of-sight angle, θ, by:[1]

$$\Phi = D \cos \theta \tag{1}$$

[1] Refraction has not been considered in this paper. See reference 12.

and the time of arrival difference is given by:

$$T_B - T_A = \Delta t = \frac{D \cos \theta}{c} \tag{2}$$

with T_B the time of arrival at antenna "B", T_A the time of arrival at antenna "A", Φ and D in meters, θ in radians, Δt in seconds, and c, the speed of light, in units of meters/second. The measurement made by the system is related to the time of arrival difference Δt. How this occurs is seen by following the antenna inputs through the simplified block diagram in Figure 2.

At antenna "A", at some instant of time the incoming signal is $\sin \psi(t)$. At that same instant of time, the observed signal at antenna "B" is:

$$\sin \psi (t - \Delta t) = \sin \left[\psi \left(t - \frac{D \cos \theta}{c} \right) \right] \tag{3}$$

For example, if the input at antenna "A" is a constant frequency sinusoid, then

$$\sin \psi (t) = \sin (2\pi f_t t) \tag{4}$$

where f_t is the frequency of emission from the satellite in Hz. This assumption neglects Doppler effects which are included in later sections. At Antenna "B":

$$\sin \psi (t - \Delta t) = \sin [2\pi f_t (t - \Delta t)] \tag{5}$$

$$\sin \psi (t - \Delta t) = \sin \left(2\pi f_t t - \frac{2\pi f_t D}{c} \cos \theta \right) \tag{6}$$

Examine the term $2\pi f_t D \cos\theta / c$. The quantity f_t/c is equal to $1/\lambda_t$ where λ_t is the wavelength of the transmitted frequency and is assumed a constant.

$$\frac{2\pi f_t D \cos\theta}{c} = \frac{2\pi}{\lambda_t} D \cos\theta \tag{7}$$

The baseline separation, D, is approximately equal to $50\lambda_t$ at a frequency f_t of 136 MHz, the nominal operating frequency of the Minitrack system. Assume for the moment that D is exactly equal to $50\lambda_t$. Then

$$\frac{2\pi}{\lambda_t} D \cos\theta = 2\pi (50) \cos\theta \tag{8}$$

Since cosine θ can vary between +1 and -1 for $0° \leq \theta \leq 180°$, the effective phase difference $(2\pi/\lambda_t)D \cos\theta$ between the two antennas "A" and "B" can vary between $+50\ (2\pi)$ and $-50\ (2\pi)$ radians. The Minitrack system (and any interferometer system operating with a narrow spectrum emission) cannot resolve the multiples of 2π with only the two antennas, fine antenna "A" and fine antenna "B", spaced apart many wavelengths of λ_t. It should be noted that other pairs of Minitrack antennas, spaced smaller distances apart, resolve the integral number of 2π radians change, and the pair of fine antennas measures the excess angle remaining.

For the moment assume no restriction on the phase function $\psi(t)$. At antenna "A" output we have

$$\sin \{\psi(t) + U[\theta(t)]\} \tag{9}$$

where $U[\theta(t)]$ is the phase change to $\psi(t)$ caused by the phase pattern of antenna "A" looking in the direction θ. Of course, θ is a time varying function. Similarly at antenna "B" output we have:

$$\sin \{\psi(t - \Delta t) + V[\theta(t - \Delta t)]\} \tag{10}$$

but note here the phase change at antenna "B", $V[\theta]$ differs from the phase change $U[\theta]$ because of the time of arrival difference, Δt.

A reference frequency of 100 Hz, f_r, is mixed with the antenna "B" signal to produce a signal at point B in Figure 2:

$$\sin \{\psi(t - \Delta t) + V[\theta(t - \Delta t)] + 2\pi f_r t\} \tag{11}$$

No change is made to the antenna "A" signal and at point A in Figure 2, we have,

$$\sin \{\psi(t) + U[\theta(t)]\} \tag{12}$$

The signals at points B and A are summed:

$$\sin \{\psi(t - \Delta t) + V[\theta(t - \Delta t)] + 2\pi f_r t\} + \sin \{\psi(t) + U[\theta(t)]\} =$$

$$2 \cos \frac{1}{2} \{2\pi f_r t + \psi(t - \Delta t) - \psi(t) + V[\theta(t - \Delta t)] - U[\theta(t)]\}$$

$$\times \sin \frac{1}{2} \{2\pi f_r t + \psi(t - \Delta t) + \psi(t) + V[\theta(t - \Delta t)] + U[\theta(t)]\} \tag{13}$$

The appearance of this signal is shown in Figure 3 as "Summer Output." From Equation (13), the envelope of the summed signals B + A is seen to carry angle of arrival information. In Figure 3, Δt was made zero and $V[\theta] = U[\theta]$. The envelope is amplitude detected in a half wave rectifier to recover (see Figure 3):

$$\cos \frac{1}{2} \{2\pi f_r t + \psi(t - \Delta t) - \psi(t) + V[\theta(t - \Delta t)] - U[\theta(t)]\} \qquad (14)$$

The postdetection filter output (the subject of this paper) recovers

$$\cos \{2\pi f_r t + \psi(t - \Delta t) - \psi(t) + V[\theta(t - \Delta t)] - U[\theta(t)]\} \qquad (15)$$

In Equation (15) the nominal frequency of the filter output is 100 Hz, the frequency of the reference signal; the $\psi(t - \Delta t) - \psi(t)$ phase term carries (ambiguous) information about the angle of arrival θ; and the $V[\theta(t - \Delta t)] - U[\theta(t)]$ represents the phase term resulting from the antenna phase perturbations. In theory, these antenna phase perturbations are predetermined by aircraft flyover calibrations.

The significance of Equation (15) is the conversion of the phase difference between the two antennas $\psi(t - \Delta t) - \psi(t)$, from a phase difference at a nominal frequency of 136 MHz, to a phase difference at a frequency of 100 Hz. This amounts to a scaling of time of approximately 136 MHz/100 Hz, or exactly f_t / f_r for a constant frequency f_t.

At the postdetection filter output, for each negative going zero crossing of the filtered/detected signal, a stop pulse is generated to control the stop time of a counter which counts a frequency of 100 kilohertz. The start pulse is generated by each[2] negative going zero crossing of the reference frequency. Hence the Minitrack measurement, C_0, is the number of cycles of f_c, 100 kHz, which occur between the negative going zero crossing of the 100 Hz reference frequency, f_r, and the succeeding negative going zero crossing of the detected signal (in the time interval, δ seconds). See Figure 4 for a pictorial representation of this measurement and its ambiguity.

In Equation (15), define $\phi(t)$ as the following quantity:

$$\phi(t) = \{\psi(t - \Delta t) - \psi(t) + V[\theta(t - \Delta t)] - U[\theta(t)]\} \tag{16}$$

Now assume that:[3]

$$U[\theta(t)] = V[\theta(t - \Delta t)] \tag{17}$$

The effect of this assumption will be discussed under filter response to satellite dynamics. Then

$$\phi(t) = \{\psi(t - \Delta t) - \psi(t)\} \tag{18}$$

[2] In present practice, the sample rate is controlled by deleting pairs of start/stop pulses. For example a 5/sec sample rate would utilize each 20th pair of start/stop pulse to control the counter. For all other pairs the counter would be inactive.

[3] This is equivalent to saying that $V[\theta(t - \Delta t)] - U[\theta(t)] = K(\theta)$ where $K(\theta)$ is an exactly known precalibrated function.

When Figure 4 is examined, it becomes apparent that $\phi(t)$, the total phase difference, is not utilized for the system measurement. Instead, the remainder of $\phi(t)$ after division by 2π radians, determines the measured quantity. Define a quantity

$$\phi(t), \text{ modulo } 2\pi = \phi(t)_{\text{Mod } 2\pi} \tag{19}$$

which is the division of $\phi(t)$ by 2π radians and the remainder is the result, $\phi(t)_{\text{Mod } 2\pi}$. Hence the input to the stop pulse generator is

$$\cos\left[2\pi f_r t + \phi(t)_{\text{Mod } 2\pi}\right] \tag{20}$$

and negative going zero crossings (stop pulses) occur at

$$2\pi f_r t_{zc_S} + \phi(t)_{\text{Mod } 2\pi} = (4k+1)\frac{\pi}{2} \qquad k = 0, 1, 2, \ldots \tag{21}$$

$$t_{zc_S} = \frac{(4k+1)\frac{\pi}{2} - \phi(t)_{\text{Mod } 2\pi}}{2\pi f_r} \tag{22}$$

where t_{zc_S} are the negative going zero crossings of the signal.

The input to the start pulse generator is $\cos(2\pi f_r t)$ and start pulses occur at:

$$2\pi f_r t_{zc_R} = (4k+1)\frac{\pi}{2} \qquad k = 0, 1, 2 \tag{23}$$

$$t_{zc_R} = \frac{(4k+1)\frac{\pi}{2}}{2\pi f_r} \tag{24}$$

where t_{zc_R} are the negative going zero crossings of the reference.

The difference in the time of negative going zero crossings is Equation (22) minus Equation (24), defined by the symbol δ in seconds ($\delta \neq \Delta t$, see Figure 4 for illustration, when f_t is a constant).

$$\delta = \frac{(4k+1)\frac{\pi}{2} - \phi(t)_{\text{Mod } 2\pi} - (4k+1)\frac{\pi}{2}}{2\pi f_r} \tag{25}$$

$$\delta = -\frac{\phi(t)_{\text{Mod } 2\pi}}{2\pi f_r} = \frac{[\psi(t) - \psi(t-\Delta t)]_{\text{Mod } 2\pi}}{2\pi f_r} \tag{26}$$

In reference to Figures 2 and 4, it can be seen that δ in seconds is:

$$\delta = \frac{C_0}{f_c} \tag{27}$$

where C_0 is the number of cycles, or counts, of the counting frequency, f_c, and $f_c = 100$ kHz.

Assume that the input to antenna "A" is a constant frequency sinusoid, that is Equation (4):

$$\sin \psi(t) = \sin(2\pi f_t t) \tag{4}$$

and the input to antenna "B" becomes:

$$\sin \psi(t-\Delta t) = \sin\left(2\pi f_t t - \frac{2\pi f_t D \cos\theta}{c}\right) \tag{6}$$

Further assume Equation (17) and see footnote 3:

$$U\,[\theta\,(t)] = V\,[\theta\,(t - \Delta t)] \tag{17}$$

With these assumptions, Equation (26) becomes:

$$\delta = \frac{C_0}{f_c} = \frac{\left[2\pi f_t\, t - \left(2\pi f_t\, t - 2\pi f_t \frac{D\cos\theta}{c}\right)\right]_{\text{Mod } 2\pi}}{2\pi f_r} \tag{28}$$

$$\delta = \frac{C_0}{f_c} = \frac{1}{2\pi f_r}\left[\frac{2\pi f_t}{c} D\cos\theta\right]_{\text{Mod } 2\pi} \tag{29}$$

From Figure 4, it may be seen that for a constant frequency sinusoid,

$$\frac{f_t}{f_r}\Delta t = K\frac{1}{f_r} + \delta \tag{30}$$

where K is the ambiguity number determined by the closer spaced Minitrack antenna pairs. From Equation (2)

$$\cos\theta = \frac{c}{D}\Delta t \tag{31}$$

$$\cos\theta = \frac{c}{D}\left[\frac{K}{f_t} + \frac{f_r}{f_t}\frac{C_0}{f_c}\right] \tag{32}$$

For later reference, it is appropriate here to examine magnitudes of typical error sources in the measurement. The first source of error to be shown is the quantization error of the measurement counter. From Equation (32),

$$- \sin \theta \, d\theta = \frac{c}{D} \frac{f_r}{f_t} \frac{1}{f_c} \, d C_0 \tag{33}$$

Baseline separation $D \approx 50 \lambda_t$, and around station zenith $\sin \theta \simeq 1$, so that Eq. (33) is

$$d\theta \simeq - \frac{f_r}{50 f_c} \, d C_0 \tag{34}$$

In the present system f_c is 100 kHz, f_r is 100 Hz, and dC_0, the quantization of the count is 1.

$$d\theta \Big|_{dC_0 = 1 \text{ count}} \simeq - 2 (10^{-5}) \text{ radians} \tag{35}$$

Equation (35) expresses the angular error in the line-of-sight for a one count error in the measurement count. Equation (35) expressed in arc seconds is:

$$d\theta \Big|_{dC_0 = 1 \text{ count}} \simeq - 4.1 \text{ arc seconds} \tag{36}$$

and reflects the maximum error in the present Minitrack system due to quantization of the measurement.

The second source of error considered here is the uncertainty or bias in the transmission frequency of the satellite, f_t. (See Appendix A for the insignificant error caused by time varying f_t). From equation (32)

$$-\sin\theta\, d\theta = \frac{c}{D}\left[K + \frac{f_r C_0}{f_c}\right]\left[-\frac{1}{f_t^2}\right] df_t \tag{37}$$

Again baseline separation $D \simeq 50\,\lambda_t$; at zenith $K = 0$, and at $\theta = 85°$, $K = 4$,

$$d\theta\Big|_{\substack{\theta=90° \\ C_0=999}} \approx .02\,\frac{df_t}{f_t} \text{ radians} \tag{38}$$

$$d\theta\Big|_{\substack{\theta=85° \\ C_0=999 \\ K=4}} \simeq 0.1\,\frac{df_t}{f_t} \text{ radians} \tag{39}$$

$$d\theta\Big|_{\substack{\theta=90° \\ C_0=999}} \approx 4.1\,(10^3)\,\frac{df_t}{f_t} \text{ arc seconds} \tag{40}$$

$$d\theta\Big|_{\substack{\theta=85° \\ C_0=999 \\ K=4}} \approx 2.1\,(10^{-4})\,\frac{df_t}{f_t} \text{ arc seconds} \tag{41}$$

The restriction of θ in Equations 38-40, is made because the main antenna lobe of the fine Minitrack antenna is approximately 10 degrees wide. (See reference 3). Measurement data are taken as the satellite traverses this 10 degree beamwidth. Assume that df_t is 1 kHz and that f_t = 136 MHz. Then

$$d\theta\Big|_{\substack{\theta=85° \\ C_0=999 \\ \Delta f_t = 1\,kHz}} \simeq .15 \text{ arc sec} \tag{42}$$

$$d\theta\Big|_{\substack{\theta = 90° \\ C_0 = .999 \\ \Delta f_t = 1\,k\,Hz}} \simeq .03 \text{ arc sec} \tag{43}$$

Equations (42) and (43) express the maximum error in the present Minitrack system due to an unknown offset of the satellite transmitted frequency (constant doppler or bias offset) for the conditions noted. This error source must be termed insignificant when viewed against other error sources (also see Appendix A for the smaller error caused by doppler rate in f_t).

The third and major source of error in the Minitrack system (and any interferometer system) are unknown path delays in the measurement system, especially the antennas, prior to summing of the signals. Again refraction has not been made a consideration here. See Figure 2 for an illustration of unknown path delay errors. Assume that there exists an unknown delay of τ seconds in the path from antenna "A" to the summer. It follows that equation (26) becomes:

$$\delta' = \frac{[\psi(t - \tau) - \psi(t - \Delta t)]_{\text{Mod } 2\pi}}{2\pi f_r} \tag{44}$$

For a constant frequency sinusoid as system input, equation (29) becomes:

$$\delta' = \frac{C_0'}{f_c} = \frac{1}{2\pi f_r}\left[\frac{2\pi f_t D \cos\theta}{c} - 2\pi f_t \tau\right]_{\text{Mod } 2\pi} \tag{45}$$

Define:

$$\Delta\delta = \delta - \delta' \tag{46}$$

At zenith, $\theta = 90°$; $\cos\ \theta = 0$ and equation (46) is

$$\Delta\delta\Big|_{\substack{\theta = 90° \\ f_t = \text{constant}}} = \frac{1}{2\pi f_r}\left[2\pi f_t \tau\right]_{\text{Mod } 2\pi} \tag{47}$$

Assume $\tau = 1$ nanosecond $= 10^{-9}$ seconds, that is there exists an unknown or uncalibrated delay in the antenna "A" path of 10^{-9} seconds.[4] Then

$$\Delta\delta\Big|_{\substack{\theta = 90° \\ f_t = \text{constant} = 136\ \text{MHz} \\ \tau = 10^{-9}}} = \frac{.136}{f_r} \text{ seconds} \tag{48}$$

From Equation (32) we have

$$\cos\theta = \frac{c}{D}\left[\frac{K}{f_t} + \frac{f_r}{f_t}\delta\right] \tag{49}$$

$$-\sin\theta\, d\theta = \frac{c}{D}\frac{f_r}{f_t}\, d\delta \tag{50}$$

At zenith, and with $D = 50\lambda_t$

$$d\theta\Big|_{\theta = 90°} \approx -\frac{f_r}{50}\, d\delta \tag{51}$$

From equation (48) for

$$\theta = 90°,\ f_t = 136\ \text{MHz},\ \tau = 10^{-9}$$

[4] This is equivalent to a path length change in antenna A, its associated cabling or its electronics of 0.3 meters for a velocity of propagtion assumed equal to the speed of light, c.

$$d\delta\Big|_{\substack{\theta = 90^\circ \\ f_t = \text{constant} = 136\ \text{M Hz} \\ \tau = 10^{-9}}} = \Delta\delta\Big|_{\substack{\theta = 90^\circ \\ f_t = \text{constant} = 136\ \text{M Hz} \\ \tau = 10^{-9}}} = \frac{.136}{f_r}\ \text{seconds} \qquad (52)$$

and

$$d\theta\Big|_{\substack{\theta = 90^\circ \\ f_t = 136\ \text{M Hz} = \text{constant} \\ \tau = 10^{-9}}} \approx -\frac{.136}{50}\ \text{radians} \qquad (53)$$

$$d\theta\Big|_{\substack{\theta = 90^\circ \\ f_t = 136\ \text{M Hz} = \text{constant} \\ \tau = 10^{-9}}} = -561\ \text{arc seconds} \qquad (49)$$

This value of 561 arc seconds demonstrates the difficulty in interferometer measurement. Flyover calibrations which measure or calibrate the unknown path length delays in the system prior to combining are done periodically, annually or semiannually. To maintain an absolute pointing error of, say 6 arc seconds, the path length differences in the antenna, cables, and electronics prior to combining, must remain stable to approximately 10^{-11} seconds or an equivalent path length difference of 3 millimeters.

Historically, these Minitrack calibration numbers are stable to the order of 10 arc seconds. For example, examine graphs 1 and 2 in Reference 5, which portray the historical record of the aircraft calibrations at the Winkfield Minitrack station from 1961 to the present (20 calibration points determined over that period of time). The shifts in the calibration for the antenna, cables, etc., for the six month period between August 1969 and February 1969 were as follows (4 arc seconds $\approx$ 1 count)

EAST-WEST FINE EQUATORIAL	-24 arc seconds
NORTH-SOUTH FINE EQUATORIAL	+ 8 arc seconds
EAST-WEST FINE POLAR	- 8 arc seconds
NORTH-SOUTH FINE POLAR	0 arc seconds

In addition, over the 9 year span of calibration, the following maximum spreads have been observed for the calibration numbers at the Winkfield station (4 arc seconds $\simeq$ 1 count):

EAST-WEST FINE EQUATORIAL	96 arc seconds
NORTH-SOUTH FINE EQUATORIAL	60 arc seconds
EAST-WEST FINE POLAR	52 arc seconds
NORTH-SOUTH FINE POLAR	48 arc seconds

These numbers and similar numbers from other Mintrack stations are not to be construed as a criticism of the system; they are meant to demonstrate the difficulty in establishing pointing accuracies on the order of 10 arc seconds. The authors believe that 10 arc seconds is the magnitude of error which should be used for system resolution.

SATELLITE DYNAMICS

The authors are indebted to Messrs. Simas and Santarpia of GSFC for the derivation of the formulas describing the phase of the input signal related to satellite dynamics (see Reference 6). These formulas and their pictorial

representation are included in the following paragraphs. In Figure 1, Geometry of Circular Orbit, a satellite in a circular orbit at a height, h_s in meters above a spherical earth, passes directly over and parallel to the baseline separation, D in meters. r is the earth radius in meters, θ is the line-of-sight angle in radians with respect to the local horizontal, and θ is shown increasing in Figure 1. The angle α, defined as the angle between the earth radius vector $\vec{r}$ to the station and the vector to the satellite $\vec{R}$, is decreasing in Figure 1. The remaining angle, β, is decreasing with time.

$$\alpha + \beta + \left(\theta + \frac{\pi}{2}\right) = \pi \tag{50}$$

$$\dot{\alpha} + \dot{\beta} + \dot{\theta} = 0 \tag{51}$$

where the dotted quantities are the time derivatives of the respective angles in radians/sec.

$$\dot{\beta} = -\dot{\theta} - \dot{\alpha} \tag{52}$$

$$\dot{\beta} = -\dot{\theta} + \frac{v_t}{R} \tag{53}$$

since

$$\dot{\alpha} = -\frac{v_t}{R} \tag{54}$$

where v_t is the tangential velocity of the satellite along the circular path above the earth. v_t is a constant positive quantity. The rotation of the earth has been neglected here. From the law of sines

$$\frac{r}{\sin \beta} = \frac{r + h_s}{\sin \left(\theta + \frac{\pi}{2}\right)} = \frac{R}{\cos \theta} \tag{55}$$

and equation (55) becomes

$$r \cos \theta = R \sin \beta \tag{56}$$

$$\beta = \sin^{-1} \left(\frac{r}{R} \cos \theta\right) \tag{57}$$

By taking the time derivative of equation (57), one obtains:

$$\dot{\beta} = -\frac{r \dot{\theta} \sin \theta}{R \left[1 - \left(\frac{r \cos \theta}{R}\right)^2\right]^{1/2}} \tag{58}$$

One can verify the correctness of the sign associated with equation (58) in the following way:

$$r,\ R,\ \left[1 - \left(\frac{r \cos \theta}{R}\right)^2\right]^{1/2},\ \text{and}\ \sin \theta\ (0 \leq \theta \leq \pi)$$

are positive quantities. θ as shown in Figure 1, is always increasing with time, so that $\dot{\theta}$ is always positive. Hence $\dot{\beta}$ is a negative quantity which physically matches the geometrical conditions shown in Figure 1.

By equating equations (53) and (58), we obtain:

$$\dot{\theta} = \frac{\frac{v_t}{R}\left[1 - \left(\frac{r \cos\theta}{R}\right)^2\right]^{1/2}}{\left[1 - \left(\frac{r \cos\theta}{R}\right)^2\right]^{1/2} - \frac{r}{R}\sin\theta} \tag{59}$$

At $\theta = 0$ on the horizon, $\dot{\theta} = v_t/R$, and directly overhead, $\theta = \pi/2$, $\dot{\theta} = v_t/h_s$. Figure 5 shows θ, and $\dot{\theta}$, for the condition of $h_s = 100$ statute miles, the assumed worst case satellite pass. The tangential velocity in meters/second is calculated from:

$$v_t = \sqrt{\frac{\mu}{r + h_s}} \tag{60}$$

where μ is the earth's gravitational parameter, 3.986016 (10^{14}) m^3/sec^2. Time is calculated from

$$t = \frac{r + h_s}{v_t}\left[\cos^{-1}\left(\frac{r}{r + h_s}\right) - \alpha\right] \tag{61}$$

with t = 0 seconds at $\theta = 0$.

For further calculation, $\ddot{\theta}$ is required. This requires the differentiation with respect to time of equation (59).

$$\ddot{\theta} = \frac{\frac{v_t}{R}\left[1 - \left(\frac{r\cos\theta}{R}\right)^2\right]^{-1/2}\left(\frac{r}{R}\right)^2 \frac{\sin(2\theta)}{2}\dot{\theta}}{\left[1 - \left(\frac{r\cos\theta}{R}\right)^2\right]^{1/2} - \frac{r}{R}\sin\theta}$$

$$- \frac{\frac{v_t r\dot{\theta}}{R^2}\left\{\frac{r}{R}\frac{\sin(2\theta)}{2} - \cos\theta\left[1 - \left(\frac{r\cos\theta}{R}\right)^2\right]^{1/2}\right\}}{\left\{\left[1 - \left(\frac{r\cos\theta}{R}\right)^2\right]^{1/2} - \frac{r}{R}\sin\theta\right\}^2} \qquad (62)$$

From the time variation of θ, it is necessary to calculate a phase variation through the system, especially through the postdetection filter shown in Figure 2. In Figure 2 and equation (1) we have defined a length Φ where:

$$\Phi = D\cos\theta \qquad (1)$$

and Φ is the difference in path length to the two antennas. Equation (15) expressed in terms of $D\cos\theta$ is:

$$\cos\left\{2\pi f_r t + \psi\left(t - \frac{D\cos\theta}{c}\right) - \psi(t) + V\left[\theta\left(t - \frac{D\cos\theta}{c}\right)\right] - U\left[\theta(t)\right]\right\} \qquad (63)$$

which is the postdetection filter output in terms of the changing length $D \cos\theta$. It is convenient here to disregard the phase changes introduced by antenna phase patterns, but later these effects will need to be considered. Equation (63) with the simplification is:

$$\cos\left\{2\pi f_r t + \psi\left(t - \frac{D\cos\theta}{c}\right) - \psi(t)\right\} \tag{64}$$

Again assume that $\psi(t) = 2\pi f_t t$; that is, the antenna input is a constant frequency sinusoid. In the preceding section, and in Appendix A, it was shown that the system error (error in line-of-sight angle θ) is relatively insensitive to changes in f_t. With this assumption, equation (64) becomes:

$$\cos\left[2\pi f_r t + \phi(t)\right] \tag{65}$$

and expressed in terms of $D\cos\theta$, equation (65) becomes:

$$\cos\left[2\pi f_r t - \frac{2\pi f_t D\cos\theta}{c}\right] \tag{66}$$

Now $c = f_t \lambda_t$ and equation (66) is

$$\cos\left(2\pi f_r t - \frac{2\pi D}{\lambda_t}\cos\theta\right) \tag{67}$$

where

$$\phi(t) = -\frac{2\pi D\cos\theta}{\lambda_t} \tag{68}$$

and equation (68) states the change in phase of the signal (other than the linear change $2\pi f_r t$) caused by the satellite dynamics.

From equation (56)

$$\cos\theta = \frac{R}{r}\sin\beta \tag{69}$$

and

$$\phi(t) = -\frac{2\pi D}{\lambda_t}\frac{R}{r}\sin\beta \tag{70}$$

By taking the time derivative of equation (70)

$$\dot{\phi}(t) = -\frac{2\pi D}{\lambda_t}\frac{R}{r}(\cos\beta)\dot{\beta} \tag{71}$$

but from equation (53)

$$\dot{\phi}(t) = -\frac{2\pi D}{\lambda_t}\frac{R}{r}(\cos\beta)\left(-\dot{\theta} + \frac{v_t}{R}\right) \tag{72}$$

$$\dot{\phi}(t) = \frac{2\pi D}{\lambda_t}\frac{R\dot{\theta}\cos\beta}{r} - \frac{2\pi D}{\lambda_t}\frac{v_t\cos\beta}{r} \tag{73}$$

The time derivative of equation (73) is:

$$\ddot{\phi}(t) = \frac{2\pi D}{\lambda_t}\frac{\dot{\beta}\sin\beta}{r}(v_t - R\dot{\theta}) + \frac{2\pi D}{\lambda_t}\frac{R}{r}\ddot{\theta}\cos\beta \tag{74}$$

The quantity $\dddot{\phi}(t)$ is also required and a numerical differentiation was performed:

$$\dddot{\phi}(t) \approx \frac{\ddot{\phi}(t = t_2) - \ddot{\phi}(t = t_1)}{t_2 - t_1} \tag{75}$$

where the time steps $t_2 - t_1$ are equal to the time required for θ to change by 1/2 degree. This was precise enough for the purpose here.

Figures (6) and (7) show ϕ, $\phi_{\text{Modulo } 2\pi}$, $\dot{\phi}$, $\ddot{\phi}$, and $\dddot{\phi}$ for $D = 50\,\lambda_t$, and h_s = 100 statute miles. $\phi_{\text{Modulo } 2\pi}$ corresponds to equation (19) where the ambiguous measurement (to multiples of 2π) is defined. In Figure 6, $\phi_{\text{Modulo } 2\pi}$ has only 6 cycles plotted. In the approximately 37 seconds remaining before zenith, there occur 44 more cycles of 2π. At zenith $\phi_{\text{Modulo } 2\pi}$ is changing at a rate (maximum) of 15.2 radians per second, or 2.4 cycles per second. From equation (68) we have the relationship between θ, the desired result and ϕ, the phase function of the filter input signal:

$$\dot{\phi}(t) = -\frac{2\pi D}{\lambda_t} \cos\theta \tag{68}$$

For D equal to $50\,\lambda_t$

$$\phi = -100\,\pi \cos\theta \tag{76}$$

$$d\phi = 100\,\pi \sin\theta\, d\theta \tag{77}$$

Near zenith, $\sin\theta \approx 1$, and

$$d\theta\,(\text{radians}) \approx \frac{1}{100\,\pi}\, d\phi \tag{78}$$

where $d\phi$ is expressed in radians. For $d\theta$ in arc seconds:

$$d\theta \text{ (arc seconds)} \approx 657\, d\phi \tag{79}$$

SYSTEM DESIGN CONSIDERATIONS

Some comments about the signal dynamics and electronic system design are needed at this point. These comments are based upon the "worst case" assumption of a 100 statute mile high satellite passing directly over the station. Refer back to Figure 2. In this block diagram much has been eliminated for the sake of simplicity. For example, the conversion of the summed antenna A + B signals to an intermediate frequency and the filtering (predetection filtering) is not shown. No attempt was made to investigate the possible replacement of this passive filter and the amplitude detector with a coherent detector (phaselock loop). It is assumed here that for reasons such as ease of operation, the predetection filtering will remain a passive filter with a nominal 10 kHz bandwidth and this filtering is assumed to have no effect on the signal dynamics. For the post-detection filter, the signal dynamics are described by equation (68):

$$\phi(t) = -\frac{2\pi D}{\lambda_t} \cos\theta(t) \tag{68}$$

and the postdetection filter, whether active or passive must be designed for these signal dynamics. The present filter is a passive, 10 Hz (nominal) bandwidth filter, which is sufficient for the "worst case" signal dynamics shown in Figures 6

and 7. Time delay through the passive filter, as long as it remains a constant over the total bandwidth (not feasible), and over temperature and other variables, would cause no error in the system measurement.[5]

Here it will be considered that a phaselock loop filter could be built which matches as closely as possible the signal dynamics. The next section of this report will examine the phase error of a phaselock loop filter for various orders and bandwidth, and how the small but finite phase error impacts system error.

PHASELOCK LOOP RESPONSE TO SATELLITE DYNAMICS

In Figures 6 and 7, it may be seen that even for the "worst case" satellite orbit (100 statute miles directly overhead), the magnitude of the higher order derivatives of ϕ (t) diminish rapidly with order. This immediately suggests expansion of $\phi(t)$ in a Taylor series of $\phi(t)$ around any time point $t = t_0$. Thus $\phi(t)$ can be expressed in the neighborhood of t_0 as:

$$\phi(t) = \phi(t_0) + \dot{\phi}(t_0)\,[t - t_0] + \frac{\ddot{\phi}(t_0)}{2!}\,[t - t_0]^2 + \frac{\dddot{\phi}(t_0)}{3!}\,[t - t_0]^3 + \text{higher order terms.} \tag{80}$$

where the higher order terms are considered negligible here. The value $\phi(t_0)$, $\dot{\phi}(t_0)$, $\ddot{\phi}(t_0)$ and $\dddot{\phi}(t_0)$ may be read directly from Figures 6 and 7 at any arbitrary time point, t_0. For example, at $\theta = 85°$, and $t_0 = 184.4$ seconds:

[5] Mr. W. Rice of GSFC is presently investigating the variation of time delay and its effect upon present system error.

$$\phi(t_0) = -2.2 \text{ radians}^{6}. \tag{81}$$

$$\dot{\phi}(t_0) = 15.1 \ \frac{\text{radians}}{\text{sec}} \tag{82}$$

$$\ddot{\phi}(t_0) = .19 \ \frac{\text{radians}}{(\text{sec})^2} \tag{83}$$

$$\dddot{\phi}(t_0) = -0.10 \ \frac{\text{radians}}{(\text{sec})^3} \tag{84}$$

For the purpose of solving for a phaselock loop response around the time, t = 184.4 seconds, the input to the phaselock loop can be represented adequately by:

$$\phi_{IN}(t) \approx -2.2 + 15.1\, t + \frac{0.19}{2} t^2 - \frac{0.1}{6} t^3 \tag{85}$$

where $\phi_{IN}(t)$ is the input to a phaselock loop at, and around t = 184.4 seconds for the assumed "worst case" satellite orbit, h_s = 100 statute miles. In equation (85), t = 0 at t_0 = 184.4 seconds.

Table I lists the equations for solution of the error response of an acceptable third order loop (with specific characteristics defined by Reference 7). $\phi_e(t)$ describes the error response

$$\phi_e(t) = \phi_{IN}(t) - \phi_0(t) \tag{86}$$

[6] The system cannot recognize multiples of 2π radians, so that $\phi(t_0) = \phi_{\text{Mod } 2\pi}(t_0)$.

TABLE I

Equations for Error Response-Mallinckrodt Third Order Loop

$$\frac{\phi_e(s)}{\phi_{in}(s)} = \frac{s^3}{\left(s + \frac{\omega_n}{4}\right)(s + \omega_n)^2} \tag{I-1}$$

$$\omega_n \left(\frac{rad}{sec}\right) = \frac{B_L\,(Hz)}{0.743} \tag{I-2}$$

$$\phi_e(s) = \phi_{in}(s) \frac{s^3}{\left(s + \frac{\omega_n}{4}\right)(s + \omega_n)^2} \tag{I-3}$$

$$\phi_e(s) = \left[\frac{\phi}{s} + \frac{\dot{\phi}}{s^2} + \frac{\ddot{\phi}/2}{s^3} + \frac{\dddot{\phi}/6}{s^4}\right]\left[\frac{s^3}{\left(s + \frac{\omega_n}{4}\right)(s + \omega_n)^2}\right] \tag{I-4}$$

$$\phi_e(s) = \phi \frac{s^2}{\left(s + \frac{\omega_n}{4}\right)(s + \omega_n)^2} + \dot{\phi} \frac{s}{\left(s + \frac{\omega_n}{4}\right)(s + \omega_n)^2} + \frac{\ddot{\phi}}{2} \frac{1}{\left(s + \frac{\omega_n}{4}\right)(s + \omega_n)^2} +$$

$$\frac{\dddot{\phi}}{6} \frac{1}{s\left(s + \frac{\omega_n}{4}\right)(s + \omega_n)^2} \tag{I-5}$$

$$\phi_e(t) = \phi\left[\frac{1}{9} \exp\left(-\frac{\omega_n t}{4}\right) + \left(\frac{8}{9} - \frac{4\,\omega_n}{3} t\right) \exp(-\omega_n t)\right] +$$

TABLE I (Continued)

$$\dot{\phi}\left[-\frac{4}{9\,\omega_n}\exp\left(-\frac{\omega_n t}{4}\right)+\left(\frac{4}{9\,\omega_n}+\frac{4}{3}t\right)\exp\left(-\omega_n t\right)\right]+$$

$$\frac{\ddot{\phi}}{2}\left[\frac{16}{9\,\omega_n^2}\exp\left(-\frac{\omega_n t}{4}\right)+\left(-\frac{16}{9\,\omega_n^2}-\frac{4}{3\,\omega_n}t\right)\exp\left(-\omega_n t\right)\right]+$$

$$\frac{\dddot{\phi}}{6}\left[\frac{4}{\omega_n^3}-\frac{64}{9\,\omega_n^3}\exp\left(-\frac{\omega_n t}{4}\right)+\left(\frac{28}{9\,\omega_n^3}+\frac{4}{3\,\omega_n^2}t\right)\exp\left(-\omega_n t\right)\right] \quad \text{(I-6)}$$

$$\phi_e(t)=\frac{1}{9}\exp\left(-\frac{\omega_n t}{4}\right)\left[-\frac{32\,\dddot{\phi}}{3\,\omega_n^3}+\frac{8\,\ddot{\phi}}{\omega_n^2}-\frac{4\,\dot{\phi}}{\omega_n}+\phi\right]+$$

$$\frac{1}{9}\exp\left(-\omega_n t\right)\left[\frac{14\,\dddot{\phi}}{3\,\omega_n^3}-\frac{8\,\ddot{\phi}}{\omega_n^2}+\frac{4\,\dot{\phi}}{\omega_n}+8\,\phi\right]+$$

$$\frac{t}{3}\exp\left(-\omega_n t\right)\left[\frac{2\,\dddot{\phi}}{3\,\omega_n^2}-\frac{2\,\ddot{\phi}}{\omega_n}+4\,\dot{\phi}-4\,\omega_n\,\phi\right]+\frac{2\,\dddot{\phi}}{3\,\omega_n^3} \quad \text{(I-7)}$$

where $\phi_{IN}(t)$ is of the form of equation (85) with constant coefficients for t, t^2, and t^3, and $\phi_0(t)$ is the output phase corresponding to the input $\phi_{IN}(t)$. The functions of "s" shown in the table are the Laplace transforms of the input function $\phi_{IN}(t)$ and the Laplace transforms of the phaselock loop component values.

The solution for the error $\phi_e(t)$ assumes that the phaselock loop has no initial information about the input $\phi_{IN}(t)$, and that the input conditions remain over all time of the form:

$$\phi_{IN}(t) = K_1 + K_2 t + K_3 t^2 + K_4 t^3 \qquad (87)$$

where K_1, K_2, K_3, and K_4 are constants.

Even with these restrictions, the application of these methods will provide insight into the phaselock loop design requirements. Admittedly by choosing the Mallinckrodt form of the 3rd order loop, further restriction has been placed upon a 3rd order loop design, but the prior operational experience gained with this 3rd order loop (for example, the Goddard Range and Range Rate Tracking System) and its demonstrated stability, make it an acceptable potential design. The one parameter left undefined in Table I is the phaselock loop bandwidth, B_L. This is the standard symbol for the (one-sided) loop noise bandwidth, and for the purpose here will be fixed at either 10, 5, or 3 Hz, and in a few instances at 20 Hz.

In Table II, the equations for a second order phaselock loop are given, also with B_L as a variable parameter. The damping factor is fixed at $1/\sqrt{2}$. The equations are given similarly in terms of constant values for ϕ, $\dot{\phi}$, $\ddot{\phi}$ and $\dddot{\phi}$.

TABLE II

Equations for Error Response – Second Order Phaselock Loop

(Weiner Filter)

$$\frac{\phi_e(s)}{\phi_{IN}(s)} = \frac{s^2}{s^2 + 2\rho\omega_n s + \omega_n^2} \tag{II-1}$$

$$\rho = \text{damping factor} = \frac{1}{\sqrt{2}} \tag{II-2}$$

$$\omega_n \left(\frac{\text{rad}}{\text{sec}}\right) = \frac{4\sqrt{2}\, B_L\,(\text{Hz})}{3} \tag{II-3}$$

$$\phi_e(s) = \phi_{IN}(s)\, \frac{s^2}{s^2 + \sqrt{2}\,\omega_n s + \omega_n^2} \tag{II-4}$$

$$\phi_e(s) = \left[\frac{\phi}{s} + \frac{\dot{\phi}}{s^2} + \frac{\ddot{\phi}/2}{s^3} + \frac{\dddot{\phi}/6}{s^4}\right]\left[\frac{s^2}{s^2 + \sqrt{2}\,\omega_n s + \omega_n^2}\right] \tag{II-5}$$

$$\phi_e(s) = \phi\, \frac{s}{s^2 + \sqrt{2}\,\omega_n s + \omega_n^2} + \dot{\phi}\, \frac{1}{s^2 + \sqrt{2}\,\omega_n s + \omega_n^2} +$$

$$\frac{\ddot{\phi}}{2}\, \frac{1}{s\,(s^2 + \sqrt{2}\,\omega_n s + \omega_n^2)} + \frac{\dddot{\phi}}{6}\, \frac{1}{s^2\,(s^2 + \sqrt{2}\,\omega_n s + \omega_n^2)} \tag{II-6}$$

$$\phi_e(t) = \phi\left\{\exp\left(-\frac{\omega_n t}{\sqrt{2}}\right)\left[\cos\frac{\omega_n t}{\sqrt{2}} - \sin\frac{\omega_n t}{\sqrt{2}}\right]\right\} +$$

TABLE II

$$\dot{\phi}\left[\frac{\sqrt{2}}{\omega_n}\exp\left(-\frac{\omega_n t}{\sqrt{2}}\right)\sin\frac{\omega_n t}{\sqrt{2}}\right]+$$

$$\frac{\ddot{\phi}}{2}\left\{\frac{1}{\omega_n^2}\left\{1-\exp\left(-\frac{\omega_n t}{\sqrt{2}}\right)\left[\sin\frac{\omega_n t}{\sqrt{2}}+\cos\frac{\omega_n t}{\sqrt{2}}\right]\right\}\right\}+$$

$$\frac{\dddot{\phi}}{6}\left\{\frac{t}{\omega_n^2}-\frac{\sqrt{2}}{\omega_n^3}\left[1-\exp\left(-\frac{\omega_n t}{\sqrt{2}}\right)\cos\frac{\omega_n t}{\sqrt{2}}\right]\right\} \qquad \text{(II-7)}$$

$$\phi_e(t)=\frac{\dddot{\phi}}{6\,\omega_n^2}t-\frac{\dddot{\phi}\sqrt{2}}{6\,\omega_n^3}+\frac{\ddot{\phi}}{2\,\omega_n^2}+$$

$$\exp\left(-\frac{\omega_n t}{\sqrt{2}}\right)\cos\frac{\omega_n t}{\sqrt{2}}\left(\frac{\dddot{\phi}\sqrt{2}}{6\,\omega_n^3}-\frac{\ddot{\phi}}{2\,\omega_n^2}+\phi\right)+$$

$$\exp\left(-\frac{\omega_n t}{\sqrt{2}}\right)\sin\frac{\omega_n t}{\sqrt{2}}\left(-\frac{\ddot{\phi}}{2\,\omega_n^2}+\frac{\sqrt{2}\,\dot{\phi}}{\omega_n}-\phi\right) \qquad \text{(II-8)}$$

Figure 8 portrays the absolute value of phase error, $|\phi_e(t)|$, as a function of time after the initially quiescent third order loop attempts signal acquisition. In Figure 8, the satellite is at an elevation angle (interferometer angle) of 85 degrees at TIME equal to zero. The abscissa value is labelled TIME to differentiate

it from the abscissa labelled t in Figures (6) and (7). At t = 184.4 seconds in Figs. 6 and 7, TIME = 0 in Fig. 8. For TIME greater than zero in Fig. 8, the values of $\phi_{\text{Mod } 2\pi}$, $\dot{\phi}$, $\ddot{\phi}$, and $\dddot{\phi}$ are assumed to remain constant at the values for t = 184.4 seconds in Figs. 6 and 7. Absolute magnitude of ϕ_e was chosen for the ordinate of Fig. 8 to avoid positive and negative values for ϕ_e. By choosing $|\phi_e|$ as the dependent variable, the plot becomes approximately the envelope of the phase error, except at TIME very large, where it approaches $2\dddot{\phi}/3\,\omega_n^3$. Since only a finite number of values of TIME were used in the solution of $|\phi_e|$, (TIME = 0, 1/4, 1/2, 3/4, 1, 2, 3, 4, 10, 20, 100), the graph has a jagged appearance. This is caused by the oscillatory nature of ϕ_e for TIME less than approximately 2 seconds. Fig. 8 was constructed by connecting the computed values $|\phi_e|$ at TIME = 0, 1/4, 1/2, etc. with straight lines. For small values of $|\phi_e|$ corresponding to large values of TIME, this method of presentation is satisfactory. The reader should note the variation of TIME scale along the abscissa.

The four horizontal lines in Fig. 8 have the following significance: the top line shows the approximate limit for computation of error from the linear equations of Table I. Above that top line, values of ϕ_e must be qualified. For example, in Fig. 8, at TIME = 0, a phase error $|\phi_e|$ of 2.2 radians is plotted and this value lies above the approximate limit for loop acquisition. By examining the linear equation (I-7) of Table I, one sees at TIME = zero that

$$\phi_e \simeq \phi_{\text{Mod } 2\pi} \tag{77}$$

In Fig. 9, $\phi_{\text{Mod } 2\pi}$ is plotted for t between 184.2 and 186.2 seconds. At t = 184.4 seconds ($\theta = 85°$) $\phi_{\text{Mod } 2\pi}$ is -2.24 radians. From equation (77), at the time of attempted loop acquisition of 184.4 seconds, the phase error calculated from the linearized phaselock loop equation would be -2.24 radians. Of course, the linear equations do not hold for this condition. Instead a series of events occurs:

(1) An error voltage is generated in the phase detector and passed through the loop filter to drive the voltage controlled oscillator (VCO).

(2) The VCO phase and phase rates will not match the incoming signal since the initial error voltage was generated by the phase detector operating outside its linear range.

(3) The loop will continue to generate "useless" VCO control information until the difference between the input phase and the VCO phase is less than approximately one radian, so that linear operation of the loop is begun. From that time onward, the loop will tend to reduce the difference between the input phase and the VCO phase (phaselock) so long as the dynamics of this signal are within the tracking capability of the loop.

In Fig. 8, at $\theta = 85°$, one must assume that the loop is incapable of acquiring rapidly. Fortunately from an examination of Fig. 9, a mere 0.1 second later the phase input to the loop has decreased to less than 1 radian, so that linear operation of the phase detector can begin. These preceding comments are best illustrated in Fig. 10. In this figure, acquisition is begun at a time when $\phi_{\text{Mod } 2\pi}$

is zero ($\theta = 90°$). The phase error, ϕ_e, at TIME = 0 is very near zero. Except for a loop bandwidth of 3 Hz which is incapable of handling the high rates of change of phase, the phase error with time remains less than 1 radian (loop lock). The explanation for the 3 Hz bandwidth difficulty can be seen readily from Fig. 7. At $\theta = 90°$, $\dot{\phi}$ is equal to 15.2 radians/second or equivalently 2.4 cycles per second. Thus the input signal to the phaselock loop is offset in frequency by 2.4 Hz, and almost outside an assumed loop noise bandwidth of 3 Hz.

The other horizontal lines in Figs. 9 and 10 show the error in the interferometer angle θ_e in terms of ϕ_e. The values of θ_e were calculated by means of equation (79)

$$d\theta \text{ (arc seconds)} = \theta_e \approx 657\, d\phi = 657\, \phi_e \tag{88}$$

Now if one assumes that the error contribution from the phaselock loop filtering should be less than 1/10 of expected system resolution, i.e., less than 1 arc second ($\theta_e \leq 1$ arc second), it can be seen that for a bandwidth of 5 Hz a time of approximately 4 seconds is required after acquisition is attempted before the interferometer error θ_e is less than 1 arc second. This condition applies for the satellite passing zenith or near it. Similarly 2 seconds are required for the 10 Hz bandwidth and 1 second for a 20 Hz bandwidth. These seemingly small lengths of time for signal acquisition[7] are significant in terms

[7] Signal acquisition is defined here as that point in time at which θ_e is less than or equal to 1 arc second.

of the "worst case" orbit assumptions. For a 100 statute mile satellite height, the satellite remains within ±5 degrees of zenith for only 3.6 seconds. The total pass, visibility from horizon to horizon, occurs within a span of 6.2 minutes.

The reader may argue that it is not required to attempt acquisition at or near zenith. He may contend that acquisition should occur at the horizon, and by the time the satellite crosses station zenith 3.1 minutes later, the phaselock loop error should be negligible (less than 1 arc second for θ_e). The authors offer the following refutation.

Reference 3 describes the amplitude patterns of the Minitrack "fine" antenna. The amplitude pattern is seen to be fan shaped and this fan shape serves a useful purpose. In general, the satellite passing over the station does not pass exactly over the center of the station. For example, it will pass north or south of the EAST-WEST FINE EQUATORIAL antenna pair. The fan portion of the beam extends approximately 38° to the north and 38° to the south to cover this eventuality, and the satellite as it makes it traverse from west horizon to east horizon, passes through antenna sidelobes, except at approximately ±5 degrees of the station meridian. In theory, as the spacecraft signal encounters an antenna amplitude null, such as at ±5 degrees off station meridian, it sees a change of phase of 180° caused entirely by the transition from the first antenna sidelobe to the main antenna lobe. It is useful here to refer back to equation (16)

$$\phi(t) = \{\psi(t - \Delta t) - \psi(t) + V[\theta(t - \Delta t)] - U[\theta(t)]\} \qquad (16)$$

U and V have been described as the phase changes caused by antennas A and B in Fig. 2. If the two antenna phase patterns were identical and if Δt were equal to zero, V would be equal to U for any satellite dynamics and there would be no contribution to $\phi(t)$ from antenna "A" and "B" phase patterns. In practice, the phase patterns are unequal and Δt is only zero at station zenith (or station meridian for our example). For the phaselock loop which has acquired at the horizon, as it observes the signal passing from antenna lobe to antenna lobe, it will see a time varying phase perturbation caused by the Minitrack antenna pair. The authors contend that signal acquisition at the horizon is no better than signal acquisition at $\theta = 85$ degrees, since the phaselock loop will require time to reduce θ_e to less than 1 arc second for each phase transient it sees at its input, whether it is caused by signal dynamics, or antenna phase patterns.[8]

Figs. (8) and (10) covered the conditions for a Mallinckrodt third order loop serving as the postdetection filter. The next figures will show operation with a second order loop (damping factor $= 1/\sqrt{2}$) for the same conditions as for Figs. 8 and 10.

Figure 11 has acquisition attempted at $\theta = 85°$. The comments for exceeding linear operation of the loop also apply here. There will occur some small but finite time after which the loop will assume linear operation. For the second order loop, and a non-zero $\ddot{\phi}$, it may be observed from Equation (II-8) in Table II

[8] No quantitative data exists to verify this contention. A source of data could be a Minitrack station calibration wherein the calibration plane flies a pass parallel to the baseline rather than normal to it.

that ϕ_e will increase linearly with time. At a very large time, ϕ_e will be very large. Recall, however, the assumptions made about the input to the loop. $\dddot{\phi}$ by assumption is to remain constant at all time for the value encountered at θ = 85°. But for the "worst case" orbit pictured in Fig. 7, $\dddot{\phi}$ is significant only over ±20 seconds about station zenith. For the 10 Hz loop bandwidth of Fig. 11, it requires 100 seconds of constant $\dddot{\phi}$ to reach an interferometer angle error, θ_e of 3 arc seconds, but physically $\dddot{\phi}$ cannot remain a constant non-zero value over that length of time.

Acquisition times for the 10 and 5 Hz bandwidth are on the order of 1/2 and 1 second. In Fig. 12, acquisition attempted at θ = 90°, $\phi_{\text{Mod } 2\pi}$ is zero, and the acquisition time for the 10 and 5 Hz bandwidths remain near 1/2 and 1 second. The 3 Hz bandwidth is obviously too narrow as evidenced by its transient error exceeding linear loop operation. Phase error in Fig. 12 also is seen to increase linearly with time, but the same qualifications expressed in the preceding paragraph apply here as well. Third derivative of phase cannot remain significant over 100 seconds of time.

Figures 13 and 14 illustrate third order loop response for a 500 statute mile circular orbit. For this orbit the satellite remains within ±5 degrees of station zenith for 19 seconds. The entire pass from horizon to horizon occurs within a time span of 15.4 minutes. Acquisition times have not decreased notably over the 100 statute mile "worst case" orbit (Figs. 8 and 10). Here the 10 Hz loop has an acquisition time of approximately 1.5 seconds, the 5 Hz loop approximately

3 seconds, and the 3 Hz loop approximately 4.3 seconds. In Fig. 13 the values of ϕ_e above 1 radian must be qualified as in the previous figures. Note in Fig. 14 that a 3 Hz bandwidth does not exceed linear loop operation. For the 500 statute mile orbit at $\theta = 90°$, $\dot{\phi}$ is a maximum and is equal to 2.9 radians/second, or equivalently a frequency offset of 0.5 Hz. The 3 Hz bandwidth, for these conditions, does not exceed a phase error of 0.22 radians, but does have a long acquisition time, 4.3 seconds.

Figures 15 and 16 are for the condition of second order loop and the 500 statute mile satellite height, at $\theta = 85$ and $\theta = 90$ degrees. The satellite dynamics are identical for Figs. 13, 14, 15 and 16. Acquisition times are approximately 1/2, 1, and 2 seconds for the 10, 5, and 3 Hz bandwidths. Since a constant value of $\dddot{\phi}$ is assumed at time of attempted acquisition, ϕ_e increases with time. For example, in Fig. 15, the included table gives values of ϕ_e for large values of TIME; at TIME = 10,000 seconds, and $B_L = 10$ Hz, $\phi_e = 2.1\ (10^{-3})$ radians and $\theta_e \simeq 1$ arc second. It must be repeated here that a constant $\dddot{\phi}$ over 10,000 seconds is not physically realizable. The inclusion of a constant $\dddot{\phi}$ was made to show the unimportance of this source of error for the second order loop.

RECOMMENDATION FOR LOOP BANDWIDTH AND ORDER

The preceding material has defined sufficient constraints in order that a suitable design may be made for the postdetection filter of the Minitrack system. The assumptions made in this definition are repeated here:

- The "worst case" conditions occur for a circular orbit of 100 statute mile height passing directly over the Minitrack station. In this situation, satellite dynamics define maximum rates of $\dot{\phi}$, the input to the postdetection filter.

- No design changes are anticipated in the predetection filter and the amplitude detector, to reduce or increase the rates of $\dot{\phi}$ into the postdetection filter.

- Phase transients caused by input signal entrance through antenna sidelobes and nulls prevent "accurate" data taking near station horizon,[9] and force acquisition and "accurate" data taking at ±5 degrees about station meridian assuming an east-west pass.

- An error contribution of 1 arc second from the postdetection filtering is desirable and practical. This 1 arc second is 1/10 of expected overall system resolution (10 arc seconds).

- Acquisition time (reduction of θ_e to 1 arc second) can be calculated from linear phaselock theory and Taylor series expansion of $\phi(t)$, the phase function into the phaselock loop.

- $\dddot{\phi}$ cannot remain an important input to the phase lock loop over long periods of time. See Fig. 7 for illustration.

With all the preceding qualifications listed, it is recommended that a 10 Hz bandwidth, second order phaselock loop be utilized as the postdetection filter for the

9 Calibration of antenna pairs is done no lower than ±50 degrees zenith, so that data taken outside this calibration zone is questionable (see Ref. 1).

Minitrack system. Acquisition times for the "worst case" orbit conditions are on the order of 1/2 second, and the error remains well below 1 arc second in pointing angle for any reasonably assumed $\dddot{\phi}$. A 3 Hz bandwidth second order loop is inadequate for following the large $\dot{\phi}$ of the "worst case" orbit, and cannot be considered acceptable. A 5 Hz, second order loop doubles the acquisition time to approximately 1 second, or approximately 25% of the total visibility times between ±5 degrees of station zenith for the 100 statute mile satellite height.

The acquisition times for the third order Mallinckrodt loop are large fractions of the visibility times between ±5 degrees of station zenith. The advantage of the 3rd order loop lies in the reduction of error caused by $\dddot{\phi}$, but for the "worst case" orbit assumed here, $\dddot{\phi}$ is not an important factor in system error. For this reason, the 3rd order loop described in Table I is not recommended for implementation.

The reader will notice that no mention of signal to noise ratio has been made to this point. Except for the assumption of a total system resolution of 10 arc seconds, based upon repeatability of aircraft calibrations, no error contribution from noise has been calculated. System design must be based upon anticipated signal dynamics, and when the design is completed, parameters in the link calculation which affect noise errors in the system must be sized accordingly. A sample calculation will be given here in explanation of this important point.

The postdetection filter is here required to be a 10 Hz, second order loop filter from the expected satellite dynamics. Preceding the postdetection filter is an amplitude detector, with a 10 kHz filter preceding the amplitude detector. System noise figure is assumed to be 4 db, and antenna gain at ±5 degrees about zenith is approximately 15 db. If the pointing error from signal to noise consideration is required to be 1 arc second, then from Equation (88)

$$\phi_e = 1.5\,(10^{-3}) \quad \text{radians} \tag{89}$$

From linear phaselock loop theory

$$\phi_e = 1.5\,(10^{-3}) = \sqrt{\frac{N}{2S}} = \sqrt{\frac{2B_L\Phi}{2S}} \tag{90}$$

where S/N is the signal to noise power ratio into the loop, and $2B_L\Phi$ is the noise power, with Φ as noise power density. Since our recommended B_L = 10 Hz:

$$\frac{S}{N} = 2.22\,(10^5) \Rightarrow (53.5 \text{ db}) \tag{91}$$

$$\frac{S}{\Phi} = 4.44\,(10^6) \Rightarrow (66.5 \text{ db-Hz}) \tag{92}$$

where S/Φ is the required signal to noise power density ratio for a pointing error of 1 arc second.

Table III gives sample calculations for required signal input for a pointing error of 1 and 10 arc seconds. Antenna gain is given for ±5 degrees about zenith. At antenna nulls, a reduction of signal from 20 to 30 db can be expected. The amplitude detector then will see signal to noise ratios of less than one for the inputs of Table III, and signal to noise ratio at the detector output will be equal to the square of the input signal to noise ratio. Consider here that data is taken only in the main lobe, i.e. antenna gain = +15 db. For a 1,000 statute mile range to the satellite at a frequency of 136 MHz, the space loss is 139.5 db. It follows that at the satellite an effective radiated power (ERP) of +21.0 dbm is required for a 1 arc second noise error, and +1.0 dbm is required for a 10 arc second noise error. This ERP is for carrier signal only, if modulation occurs during the Minitrack measurement, the total satellite ERP must be increased to account for the power in the modulation sidebands.

Now assume that for the signal inputs of Table III, the satellite is located at an antenna null of -30 db. Table IV lists the calculations for this situation, and it is apparent that drastic changes in pointing error occur while passing through a 30 db antenna null. For the input signal level corresponding to the 1 arc second error while in the main lobe of the antenna, an error of 46.4 arc seconds occurs at the assumed 30 db antenna null. For the input signal level corresponding to the 10 arc second error, no valid measurement is obtained during the antenna null (probable phaselock loop unlock).

TABLE III

Signal to Noise Calculations – Satellite in Main Antenna Lobe

θ_e = 1 Arc Second	
Required Signal Level Into Antenna	-118.5 dbm
Minitrack Antenna Gain (Main lobe only)	+15 db
Required Signal Level Into System	-103.5 dbm
Noise Power in 10 kHz Predetection Bandwidth (System NF = 4 dB)	-130 dbm
S/N Ratio Before Amplitude Detector[10]	+26.5 db
S/N Ratio After Postdetection Filter ($2B_L$ = 20 Hz)	+53.5 db
Pointing Error	1 arc second
θ_e = 10 Arc Second	
Required Single Level Into Antenna	-138.5 dbm
Minitrack Antenna Gain (Main lobe only)	+15 db
Required Signal Level Into System	-123.5 dbm
Noise Power in 10 kHz Predetection Bandwidth (System NF = 4 dB)	-130 dbm
S/N Ratio Before Amplitude Detector[10]	+6.5 db
S/N Ratio After Postdetection Filter ($2B_L$ = 20 Hz)	+33.5 db
Pointing error	10 arc second

[10] With signal to noise ratios of greater than one into the amplitude detector, output signal to noise ratio is equal to input signal to noise ratio.

TABLE IV

Signal to Noise Calculations – Satellite in Antenna Null

Signal Input Levels Same as Table III

Assumed Signal Level into Antenna (From Table III)	-118.5 dbm
Minitrack Antenna Gain (Antenna Null)	-15 db
Signal Level into System	-133.5 dbm
Noise Power in 10 kHz Predetection Bandwidth (System NF = 4 db)	-130 dbm
S/N Ratio Before Amplitude Detector[11]	-3.5 db
S/N Ratio After Amplitude Detector (10 kHz BW)	-7.0 db
Pointing error (antenna null)	46.4 arc seconds
Pointing error (antenna main lobe)	1 arc second
Assumed Signal Level into Antenna (From Table III)	-138.5 dbm
Minitrack Antenna Gain (Antenna Null)	-15 db
Signal Level into System	-153.5 dbm
Noise Power in 10 kHz Predetection Bandwidth (System NF = 4 db)	-130 dbm
S/N Ratio Before Amplitude Detector[11]	-23.5 db
S/N Ratio After Amplitude Detector (10 kHz BW)	Below Loop
S/N Ratio After Postdetection ($2B_L$ = 20 Hz)	Threshold
Pointing error (Antenna Null)	no measurement
Pointing error (Antenna Main Lobe)	10 arc seconds

[11] With signal to noise ratios of less than one into the amplitude detector, output signal to noise ratio is equal to the square of the input signal to noise ratio.

In order to assure at least a 10 arc second error during the 30 db antenna null, the required signal level input to the antenna would be -108.5 dbm and the equivalent satellite ERP required at a range of 1000 statute miles would be +31.0 dbm or slightly over 1 watt.

The repetition here is for emphasis. Signal dynamics define system parameters such as postdetection filter maximum bandwidth and order of loop. Doppler shift and phase slope characteristics define predetection filter characteristics. Signal to noise constraints are set by maximum satellite ERP. System resolution is set independent of all the foregoing, and is strictly a function of time delay calibration and time delay variation.

Still one additional parameter remains to be chosen, and that is system data rate. The postdetection filter has been described here as a 10 Hz, second order loop, and there exists a reasonable data rate commensurate with this filter type. The following sections will concern this optimum data rate selection.

THE "GAIN" IN SIGNAL TO NOISE RATIO DUE TO LEAST SQUARES SMOOTHING OF MINITRACK DATA AT THE OUTPUT OF THE POSTDETECTION FILTER

As previously mentioned, the orbital dynamics of the satellite determine the specific type of design for the postdetection filter. Once the design has been fixed, the method or manner in which the data is processed at the output of the filter determines the sampling rate.

In this section, we will investigate the effect of least squares smoothing of Minitrack data which has been correlated by the postdetection filter. It is assumed that data with white noise having zero mean and unit standard deviation is input to the filter. At the output, the data is smoothed with a least squares straight line (it is shown later that a straight line provides a sufficiently good fit to the data for purposes of this analysis) and the value of the straight line at the midpoint is used as the "value for the data" at that particular instant of time. The standard deviation of the straight line at the midpoint is determined and the ratio of the standard deviation of the input noise to the standard deviation of the straight line at the midpoint expressed in decibels is used as a measure of the improvement or "gain" in signal to noise ratio due to the least squares smoothing process. Three types of filters are investigated – single pole, double pole, and ideal (infinitely many poles) with 3-db bandwidths of 3Hz, 5Hz, and 10Hz. Inasmuch as the transfer function of a phaselock loop can be described by an equivalent electronic circuit, (reference 8), the results of this analysis for a double pole filter can be applied directly to the equivalent second order phaselock loop recommended above (the present Minitrack system has a double pole filter with a nominal bandwidth of 10Hz).

In this analysis, we will assume the same "worst case" orbital dynamics as assumed in the previous sections hold; that is, the satellite is in a 100 statute mile circular orbit, the pass is directly overhead, and the visibility arc is 10° (± 5° about zenith). In addition it is assumed that the satellite is acquired

immediately after entering the beamwidth of the Minitrack antenna. Although there is some finite delay due to acquisition, this delay is shown to be negligible in its effect upon the "gain." (See Figure 29.)

From the orbital dynamics and geometry indicated in Figures 1 and 17, the "total visible time" T_v that the satellite is in the beamwidth of the antenna can be calculated

$$T_v = \frac{2\,\alpha}{\omega_s} \tag{93}$$

where ω_s is the angular rate of the satellite, and is equal to $\dot{\alpha}$.

$$\omega_s = \sqrt{\frac{\mu}{(r + h_s)^3}} \tag{94}$$

in radians/second and α is the central angle in radians

$$\alpha = \sin^{-1}\left\{ \frac{\cos\theta \left[-r \sin\theta + \sqrt{r^2 \sin^2\theta + h_s^2 + 2\,r\,h_s} \right]}{r + h_s} \right\} \tag{95}$$

and

μ = earth's gravitational constant

r = earth's radius

h_s = satellite height above the Minitrack station

θ = interferometer angle.

From the above, for a 10° overhead arc and a satellite in a 100 statute mile orbit and a 500 statute mile orbit T_v = 3.6 seconds and T_v = 18.9 seconds respectively.

The total number of points N during time T_v is

$$N = \frac{T_v}{\tau} \tag{96}$$

where τ = time between samples

In general, the flow of information is as shown in Figure 18.

For purposes of this analysis a least squares straight line evaluated at the center point provides a good fit to the data. This can be seen in the following sense. From Fig. 1, the measurement of phase delay is proportional to cos θ where θ is the interferometer angle. Figure 19 shows a least squares straight line fit to sin (90 - θ) from +5° to -5° where it is compared to values of sin (90 - θ). It can be seen that both curves pass through zero. Therefore in the absence of any systematic and random errors the data and the fit to the data will agree at the midpoint. It is in this sense that the straight line fit is sufficient for the purpose of this analysis. Furthermore, it is felt that the same conclusions can be drawn with a higher ordered polynomial fitted to the data over the same arc length.

In Fig. 18, assume that white noise (uncorrelated) is input to the filter and that (2n + 1) data points are available for processing (equally spaced in time from - n to + n). At the filter output the (2n + 1) data points (by using 2n + 1 points

symmetrically spaced about zero the mathematics is made simpler), are fit with a least squares straight line and the value of the straight line at the center point extracted as the value for the data at that time. The question then arises, "What 'gain' is achieved at the filter output due to least squares smoothing?"

It will be seen that the "gain" achieved is a function of the number of data points, the type of filter (single pole, double pole, ideal), the bandwidth of the filter and the sampling rate $(1/\tau)$. The number of points during a total time T_v is given by equation (96). For computation purposes, the largest number of odd points in time T_v was taken for $N = 2n + 1$.

The autocorrelation functions for the single pole, double pole, and ideal filters are respectively (references 9 and 10)

Single Pole

$$\rho_{s_i} = e^{-i\,\omega_c h} \tag{97}$$

where ω_c = 3 db angular cutoff frequency of the filter.

Double Pole

$$\rho_{d_i} = \left(\sin i\,\frac{\omega_c h}{\sqrt{2}} + \cos i\,\frac{\omega_c h}{\sqrt{2}}\right) e^{-i\,\frac{\omega_c h}{\sqrt{2}}} \tag{98}$$

and

Ideal Filter

$$\rho_{I_i} = \frac{\sin (i\,\omega_c h)}{(i\,\omega_c h)} \tag{99}$$

The autocorrelation functions above give the correlation between points spaced 0, h, 2h, . . . , (2n h) units apart. It can be seen that by decreasing the bandwidth ω_c of the filter, the correlation is increased. In equation (96) τ is the sampling interval which has the same meaning as h in equation (97), (98), and (99). Thus, by increasing the sampling rate (or equivalently decreasing the sampling interval) the correlation is also increased.

From the theory of least squares (Appendix B and reference 11) the uncertainty of a straight line at the ith data point is given by (matrix notation)

$$\sigma^2_{\bar{y}_i} = \mathbf{u}^T (\mathbf{A}^T \mathbf{A})^{-1} \mathbf{A}^T \mathbf{Q} \mathbf{A} (\mathbf{A}^T \mathbf{A})^{-1} \mathbf{u} \tag{100}$$

where

$$\mathbf{u}^T = (1 \; i \; i^2 \; . \; . \; . \; . \; i^{2n})$$

A is the matrix of normal equations, i.e.,

$$\mathbf{A}^T = \begin{pmatrix} 1 & 1 & \cdots & \cdots & 1 \\ -n & \cdots & \cdots & \cdots & n \end{pmatrix}$$

and **Q** is the covariance matrix of the input noise (at the filter outputs). For a single pole filter

$$\mathbf{Q} = \begin{pmatrix} 1 & e^{-\omega_c h} & e^{-2\omega_c h} & \cdots & e^{-2n\omega_c h} \\ e^{-\omega_c h} & 1 & e^{-\omega_c h} & \cdots & e^{-(2n-1)\omega_c h} \\ \vdots & & & & \\ e^{-2n\omega_c h} & \cdots & \cdots & \cdots & 1 \end{pmatrix} \sigma_e^2 \tag{101}$$

where σ_ϵ is the standard deviation of the white noise at the filter input.

For a single pole filter, the computations are relatively simple and the mean square error at the midpoint of the straight line (i = 0) is given by

$$\sigma^2_{\bar{y}_o} = \frac{1}{(2n+1)^2} \left\{ (2n+1) + \left(\frac{2e^{-\omega_c h}}{1 - e^{-\omega_c h}} \right) 2n - \frac{2e^{-2\omega_c h}}{(1 - e^{-\omega_c h})^2} \left(1 - e^{-2n\omega_c h}\right) \right\} \qquad (102)$$

where $\sigma_\epsilon = 1$.

For the double pole filter and ideal filter, the computation for the determination of $\sigma^2_{\bar{y}_o}$ is rather involved, since it involves the summation of ρ_{d_i} and ρ_{I_i} from 1 to (2n + 1). Therefore, these calculations were done by computer.

Results of all the computations can be seen in Figs. 20 through 32 where the "gain" due to least squares filtering (smoothing) is expressed in decibels, i.e.

$$\text{Gain} = 20 \log_{10} \left(\frac{\sigma_\epsilon}{\sigma_{\bar{y}_o}} \right) \qquad (103)$$

where $\sigma_\epsilon = 1$.

In each figure, the gain is plotted versus the sampling interval (in seconds). Figure 20 shows the effect of smoothing of uncorrelated noise for a 100 statute mile overhead orbit (total "visible" time = 3.6 seconds ±5° of zenith).

Figures 21 through 26 are for a single pole filter, the first three curves for a 100 statute mile orbit and the following three for a 500 statute mile orbit (3 Hz, 5 Hz, and 10 Hz Bandwidth). The next three figures (27, 28, and 29) pertain to a double pole filter, 100 statute mile orbit and bandwidths of 3 Hz, 5 Hz, and 10 Hz. Figures 30 through 32 are for an ideal filter, 100 statute mile orbit, and bandwidths of 3 Hz, 5 Hz, and 10 Hz.

It should be noted that the curves are jagged due to the fact that the same odd number of points are used for a range of sampling intervals.

From inspection of Figure 29, it can be seen that the effect of a loss of 0.4 seconds due to acquisition time is negligible as far as its effect upon the "gain" due to smoothing.

DISCUSSION AND RECOMMENDATION FOR SAMPLING RATE

From the curves in Figs. 20 through 32, it can be seen that the effect of correlation due to the postdetection filter is to reduce the gain achieved by the least squares smoothing process. For example, in Fig. 20, the gain due to least squares smoothing of white (uncorrelated) noise for a sampling interval of .01 seconds and a 100 statute mile circular orbit (10° zenith arc) is 25.6 db. Under the same orbital dynamics conditions and sampling rate for a 10 Hz single pole, 10 Hz double pole and 10 Hz ideal filter (infinitely many poles) the gains are respectively 20.4 db, 19.2 db, and 18.6 db (Figures 21, 27, and 30).

It can also be seen that the higher the sampling interval (the lower the sampling rate) the less the correlation between sample points and therefore the

effect of the filter in this case approaches that of white noise. Inspection of Figs. 21, 22, 23, and 27 through 32, shows that the "gain" is on the order of 5 db for sampling intervals from 0.73 seconds to 1 second (compare with Fig. 20)

It is important to mention again that the choice of a particular type of post detection filter (e.g. single pole, double pole, ideal) as well as the filter bandwidth should not be made on the basis of least squares smoothing, but should depend upon requirements imposed on the system by satellite orbital dynamics as discussed previously. For example, referring to Figs. 23, 29, and 32 (100 statute mile orbit, 10 Hz single pole, double pole and ideal filter) for a sampling interval of 0.01 seconds (100 samples/second rate) the gains are respectively 20.4 db, 19.2 db, and 18.6 db; for a 0.05 second interval the gains are 18.2 db, 17.7 db, and 18.5 db; while for 0.1 seconds the respective gains are 15.4 db, 15.6 db, and 15.4 db. Thus for a fixed bandwidth and sample rate, much higher than the bandwidth, there is little difference among the 3 filter designs-less than a db for sampling intervals in the range of 0.05 to 0.1 seconds.

A question which arises is "For a fixed filter design such as a double pole filter, can anything be gained by increasing the bandwidth?"

At first glance, it would seem that this is the case. However, whenever the bandwidth is increased, the noise power increases in direct proportion (reference 9). This is shown in Fig. 33, which is a plot of the degradation in db due to an

increased bandwidth. As an example, doubling the bandwidth results in a loss of 3 db. Referring to Figs. 31 and 32 for a sampling interval from 0.05 to 0.1 seconds, a gain of approximately 3 db is shown from the curves. Therefore, the effective enhancement of the signal to noise ratio due to least squares smoothing in going from 5 to 10 Hz has been offset by a degradation in noise due to the increased bandwidth.

From the above, it can be concluded that the value of the least squares smoothing lies in choosing a range of sampling rates to achieve maximum gain for a fixed filter design. Thus for the 10 Hz double pole filter design recommended in the previous section, it appears that a sample rate of from 10 to 20/sec will provide sufficient "gain" while keeping the data handling at a minimum.

CONCLUSIONS

A study of the Minitrack System, especially in the area of proposed changes to the postdetection filter, was undertaken in support of a potential "renovation" of the NASA "workhorse". Proposed here as a suitable replacement for the present, double pole, 10 Hz bandwidth, postdetection filter is a 10 Hz noise bandwidth, second order phaselock loop filter. This proposed filter adequately meets the requirement for rapid data taking under the worst case condition of a satellite in a circular orbit 100 statute miles above the Minitrack Antenna pairs.

Minitrack data rate selection is based upon the postdetection filter design and that rate is determined from the following considerations:

(1) For a sampling rate greater than the bandwidth of the postdetection filter the effect of correlated noise (as opposed to white noise) in the Minitrack data at the filter output is a reduction in "gain" in signal to noise ratio achieved by least squares smoothing.

(2) The choice of a filter design cannot be made on the basis of the "gain" due to smoothing at the filter output for the following reasons:

   (a) For a given bandwidth and sampling rate greater than the bandwidth there is little difference in the "gain" achieved by smoothing for a single pole, double pole, and ideal filter (an infinite number of poles).

   (b) For a filter with a fixed number of poles and sampling rate much greater than the bandwidth although there is an "apparent gain" from the smoothing process by increasing the bandwidth, this gain is offset by a loss due to the fact that the system noise has increased proportionate to the increase of bandwidth.

(3) For the 10 Hz equivalent double pole filter mentioned above, a sampling rate in the range of 10 to 20 samples per second provides a sufficiently high "gain" when its output is smoothed while still keeping the data handling problem at a minimum level.

ACKNOWLEDGMENTS

This study was initiated and stimulated by numerous discussions with Messrs. V. R. Simas and D. E. Santarpia of the Advanced Development Division. Mr. Simas is presently providing recommendations to the Tracking and Data Systems Directorate for the Development of a second generation Minitrack system.

REFERENCES

1. Marsh, J. G., Doll, Jr. C. E., Sandifer, R. J., and Taylor, W. A., "Intercomparison of the Minitrack and Optical Tracking Networks Using GEOS I Long-Arc Orbital Solutions," NASA TN D-5337 (February 1970).

2. Watkins, Edward R., Jr., Preprocessing of Minitrack Data. NASA TN D-5042, May 1969.

3. Lantz, Paul A., and Thibodeau, George R., NASA Space Directed Antennas. NASA GSFC X-525-67-430, September 1967.

4. Rice, William M., A Review of NASA Minitrack Data Time-Tagging. NASA GSFC X-551-70-41, February 1970.

5. Dunivant, R., and Casto, J., Aircraft Calibration of Winkfield Minitrack. RCA Memorandum to J. D. Oosterhout, GSFC Code 514, 21 August 1969.

6. Simas, V. R., and Santarpia, D. E., Data Filtering for the New Minitrack System. NASA GSFC X-523-70-207, May 1970.

7. Mallinckrodt, A. J., Passive Ranging Doppler System. No. 961-R1, Phase A Completion Report, Ballistic Research Laboratory, 2 November 1953.

8. Gardner, Floyd M., "Phaselock Techniques," John Wiley and Sons, Inc., New York (1966).

9. Schwartz, M., "Information Transmission, Modulation, and Noise; A Unified Approach to Communication," New York: McGraw-Hill, 1959.

10. Kruger, B., "Effects of Correlated Noise with Application to Apollo Tracking Problems," NASA TN D-4121 (GSFC), February 1968.

11. Kendall, M. G., and Stuart, A., "The Advanced Theory of Statistics," Vol. 2, Hafner Publishing Company, N. Y. (1967).

12. Schmid, P. E., NASA Minitrack Interferometer Refraction Corrections. NASA GSFC X-551-69-434, October 1969.

APPENDIX A

Negligibility of Spacecraft Frequency Rate in Pointing Error Analysis

The text of the report considered the error from uncertainty in the spacecraft transmitted frequency, and for a constant uncertainty in the transmitted frequency (equivalent to a constant doppler) of 1 kilohertz, the error was shown to be negligible. Here we will show the insignificant contribution to system error from expected rate of change of received spacecraft frequency.

In the assumed "worst case" circular orbit, 100 statute mile height, the range to the satellite can be calculated from:

$$\text{RANGE} = \sqrt{R^2 + r^2 - 2\,R\,r\,\cos\,\alpha} \tag{A-1}$$

Rate of change of range can be calculated as

$$\text{RANGE RATE} = -\frac{r\,v_t}{\text{RANGE}}\,\sin\,\alpha \tag{A-2}$$

and the time derivative of range rate can be computed from:

$$\text{RANGE RATE RATE} = \frac{r\,v_t}{(\text{RANGE})^2}\left[\frac{(\text{RANGE})\,v_t}{R}\,\cos\,\alpha + \frac{\sin\,\alpha}{\text{RANGE RATE}}\right] \tag{A-3}$$

The corresponding doppler frequency and doppler frequency rate can be calculated approximately from:

$$\text{DOPPLER FREQUENCY} = f_d \approx -\frac{(\text{RANGE RATE})}{c} f_t \tag{A-4}$$

$$\text{DOPPLER FREQUENCY RATE} = \dot{f}_d \approx -\frac{(\text{RANGE RATE RATE})}{c} f_t \tag{A-5}$$

For the worst case orbit, f_d varies from 3.5 kilohertz at station horizon to 300 Hz at θ equal 85° and 0 at zenith. $\dot{f}_d$ varies from zero at the horizon to -167 Hz/sec at θ equal to 85° and -169 Hz/sec at zenith.

Recall the expression for the measurement δ where

$$\delta = \frac{C_o}{f_r} = \frac{[\psi(t) - \psi(t - \Delta t)]_{\text{Mod } 2\pi}}{2\pi f_r} \tag{A-6}$$

All symbols are defined in the text of the report. Consider that

$$\psi(t) = 2\pi f_t(t)\, t \tag{A-7}$$

that is the received frequency at antenna "A" and "B" is a function of time. Express $f_t(t)$ as a Taylor series expansion about t = 0, the arbitrary reference time at antenna "A":

$$f_t(t) = f_t(0) + \dot{f}_t(0)\, t + \ddot{f}_t(0)\, t^2 + \ldots \tag{A-8}$$

The reference time is arbitrary because the system concerns itself strictly with the frequency at antenna "A" at one instant of time and the frequency received only Δt seconds before at antenna "B". Thus

$$\psi(t) = 2\pi f_t(0)\, t + 2\pi \dot{f}_t(0)\, t^2 + 2\pi \frac{\ddot{f}_t}{2}(0)\, t^3 + \cdots \qquad \text{(A-9)}$$

Similarly

$$\psi(t-\Delta t) = 2\pi(t-\Delta t)\left\{f_t(0) + \dot{f}(0)\,[t-\Delta t]^2 + \frac{\ddot{f}(0)}{2}[t-\Delta t]^2 + \cdots\right\} \qquad \text{(A-10)}$$

and

$$[\psi(t) - \psi(t-\Delta t)]_{\text{Mod } 2\pi} = \left\{2\pi f_t(0)\,\Delta t + 2\pi \dot{f}_t(0)\,\Delta t\,[2t-\Delta t] + \right.$$

$$\left. \frac{2\pi \ddot{f}_t(0)}{2}\,\Delta t\,[(t-\Delta t)^2 + t^2 + t(t-\Delta t)] \cdots + \right\}_{\text{Mod } 2\pi} \qquad \text{(A-11)}$$

We will consider here that $\ddot{f}_t(0)$ and all higher order derivation of f_t at the reference time of zero are zero and equation (A-11) becomes:

$$[\psi(t) - \psi(t-\Delta t)]_{\text{Mod } 2\pi} = 2\pi\,[f_t(0)\,\Delta t + \dot{f}_t(0)\,\Delta t\,(2t-\Delta t)]_{\text{Mod } 1} \qquad \text{(A-12)}$$

Mod 1 means the fractional part of the bracket left after division by 1. For example

$$[5.1]_{\text{Mod } 1} = .1 \qquad \text{(A-13)}$$

The first term of the bracket contains the desired information

$$f_t(0)\,\frac{D\cos\theta}{c} \tag{A-14}$$

while the second term carries the error due to a non-zero $\dot{f}_t(0)$

$$\dot{f}_t(0)\,\frac{D\cos\theta}{c}\left[2t - \frac{D\cos\theta}{c}\right] \tag{A-15}$$

The maximum value of (A-15) occurs for the greatest time difference between arrival at the two antennas, where $t = \Delta t$, and equation (A-15) becomes

$$\dot{f}_t(0)\left(\frac{D\cos\theta}{c}\right)^2 \tag{A-16}$$

The maximum value of $\dot{f}_t(0)$ is -169 Hz/second at zenith for the assumed "worst case" orbit so that (A-16) is

$$-169\left(\frac{D\cos\theta}{c}\right)^2 \tag{A-17}$$

The ratio of this undesired term (A-17) to the desired term (A-14) is:

$$-\frac{169\left(\frac{D\cos\theta}{c}\right)^2}{f_t(0)\,\frac{D\cos\theta}{c}} = -\frac{169\,(D\cos\theta)}{c\,f_t(0)} \tag{A-18}$$

For $D = 50\ \lambda_t$, A-18 becomes

$$\left| -\frac{(169)\ (50)\ \cos\theta}{f_t^2\ (0)} \right| \leq 4.5\ (10^{-13}) \qquad \text{(A-19)}$$

The pointing error from this type of error source is always less than $2\ (10^{-5})$ arc seconds.

APPENDIX B

The Uncertainty of a Least Squares Straight Line at the Center Point For Data Correlated by a Single Pole Filter

Assume (2n + 1) observed values y_i at equally spaced time intervals (normalized to length 1 without loss of generality). A first degree polynomial

$$\bar{y}_i = a_0 + a_1 i \tag{B-1}$$

$$(i = -n, -(n-1), \ldots, (n-1), n)$$

is then fit to the data by the method of least squares. Equation (B-1) can be written in matrix notation

$$\mathbf{Y} = \mathbf{A}\,\mathbf{X} \tag{B-2}$$

where

$$\mathbf{Y} = \begin{pmatrix} y_{-n} \\ \cdot \\ \cdot \\ \cdot \\ y_n \end{pmatrix}, \quad \mathbf{A} = \begin{pmatrix} 1 & -n \\ \cdot & \cdot \\ \cdot & \cdot \\ \cdot & \cdot \\ 1 & n \end{pmatrix}, \quad \mathbf{X} = \begin{pmatrix} a_0 \\ a_1 \end{pmatrix}$$

From the least squares theory the solution $\vec{\mathbf{X}}$ for $\mathbf{X}$ is given by(*)

$$\vec{\mathbf{X}} = (\mathbf{A}^T \mathbf{A})^{-1} \mathbf{A}^T \mathbf{Y} \tag{B-3}$$

*$\mathbf{A}^T$ is the transpose of the matrix $\mathbf{A}$ and $(\mathbf{A}^T \mathbf{A})^{-1}$ is the inverse of $(\mathbf{A}^T \mathbf{A})$.

which has the covariance matrix

$$P = (A^T A)^{-1} A^T Q A (A^T A)^{-1} \tag{B-4}$$

where Q is the covariance matrix of the noise on the data.

The variance of the straight line in (B-1) can be written as

$$\sigma^2_{\overline{y}_i} = \sigma^2_{a_0} + 2 i \sigma_{a_0 a_1} + i^2 \sigma^2_{a_1} \tag{B-5}$$

or in matrix notation

$$\sigma^2_{\overline{y}_i} = u^T (A^T A)^{-1} A^T Q A (A^T A)^{-1} u \tag{B-6}$$

where

$$u = \begin{pmatrix} 1 \\ i \end{pmatrix}$$

and $\sigma^2_{a_0}$ is the variance of a_0, $\sigma_{a_0 a_1}$, is the covariance between a_0 and a_1, and $\sigma^2_{a_1}$ is the variance of a_1.

The autocorrelation function for a single pole filter is from references 8 and 9 given by

$$R(\tau) = e^{-\omega_c |\tau|} \tag{B-7}$$

where ω_c is the 3-db angular cutoff frequency of the filter. If h is the sampling interval then

$$\rho_i = e^{-i\omega_c h} \qquad (i = -n, \ldots, n) \tag{B-8}$$

gives the coefficient of correlation between data points spaced ih sampling intervals apart.

For white (uncorrelated) noise in the data at the input to the filter having zero mean and unit variance, the covariance matrix Q at the output of the filter will be

$$Q = \begin{pmatrix} 1 & e^{-h\omega_c} & e^{-2h\omega_c} & e^{-2nh\omega_c} \\ e^{-h\omega_c} & 1 & e^{-h\omega_c} & e^{-2(n-1)h\omega_c} \\ \cdots & \cdots & \cdots & \cdots \\ e^{-2nh\omega_c} & & e^{-(n-1)h\omega_c} & 1 \end{pmatrix} \tag{B-9}$$

Performing the necessary matrix operations indicated in (B-6) and letting $i = 0$ (midpoint)

$$\sigma^2_{\bar{y}_o} = \left(\frac{1}{2n+1}\right)^2 \left\{(2n+1) + \left(\frac{2e^{-h\omega_c}}{1 - e^{-h\omega_c}}\right) 2n - \frac{2e^{-2h\omega_c}}{(1 - e^{-h\omega_c})^2}\left(1 - e^{-2nh\omega_c}\right)\right\} \tag{B-10}$$

which gives mean square error of the straight line at the center point. The uncertainty of the straight line at the center is the square root of (B-10)

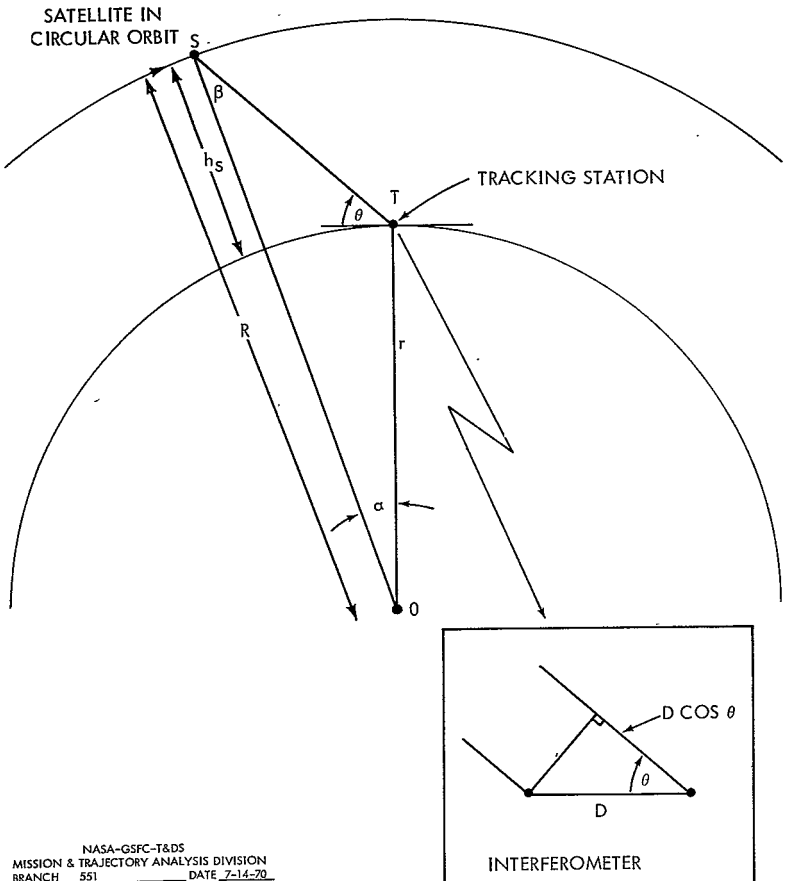

Figure 1. Geometry of Circular Orbit

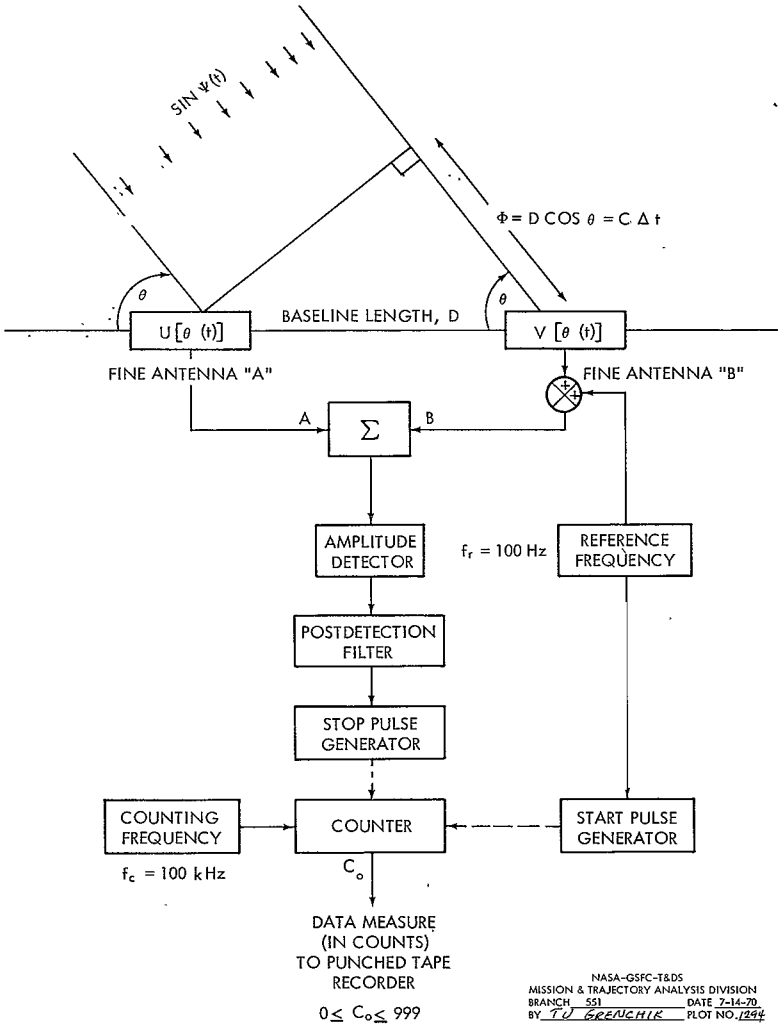

Figure 2. Simplified Block Diagram of Minitrack System

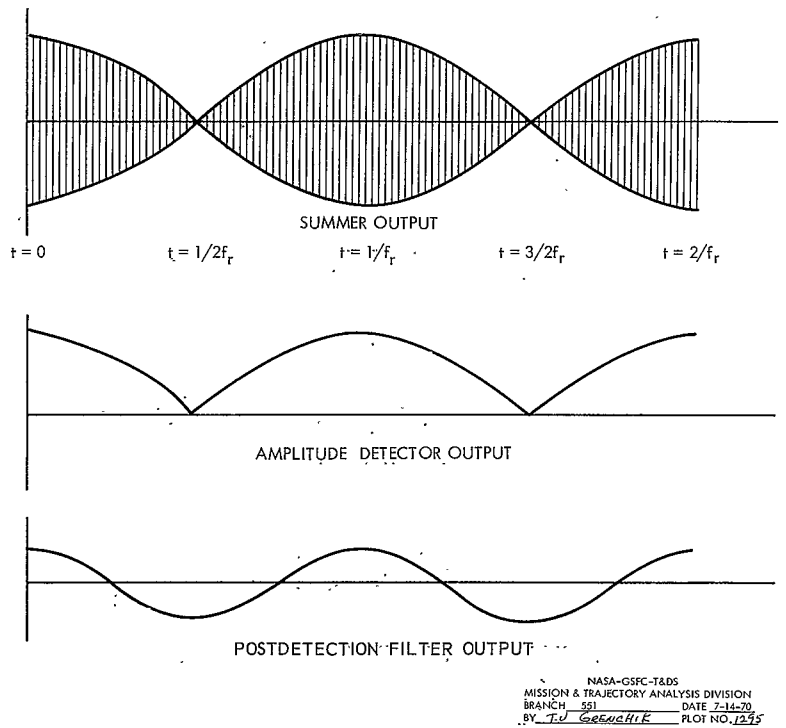

Figure 3. Waveforms in Minitrack Detection System

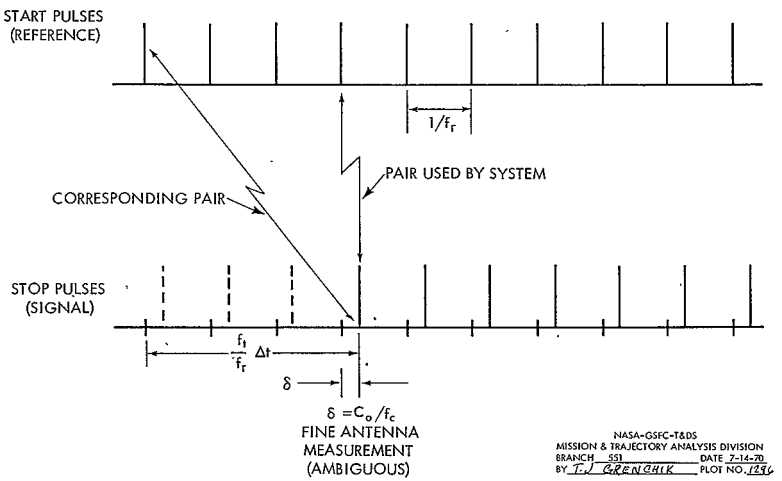

Figure 4. Time Relationships of Start/Stop Pulses For Constant Frequency Input f_t

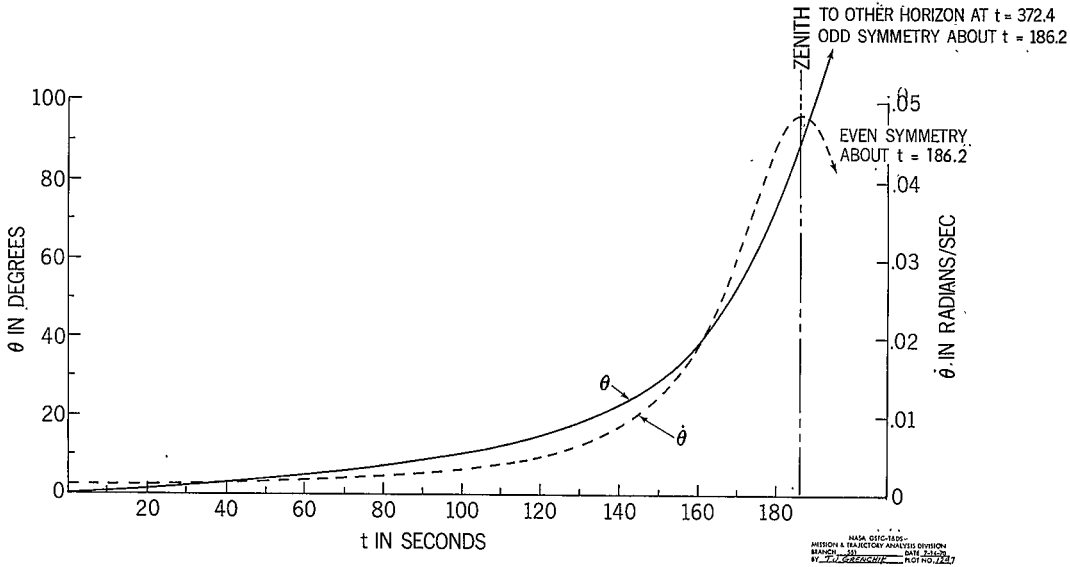

Figure 5. Minitrack Station Line of Sight Angle, θ and Rate of Change of Angle, $\dot{\theta}$, h_s = 100 Statute Miles

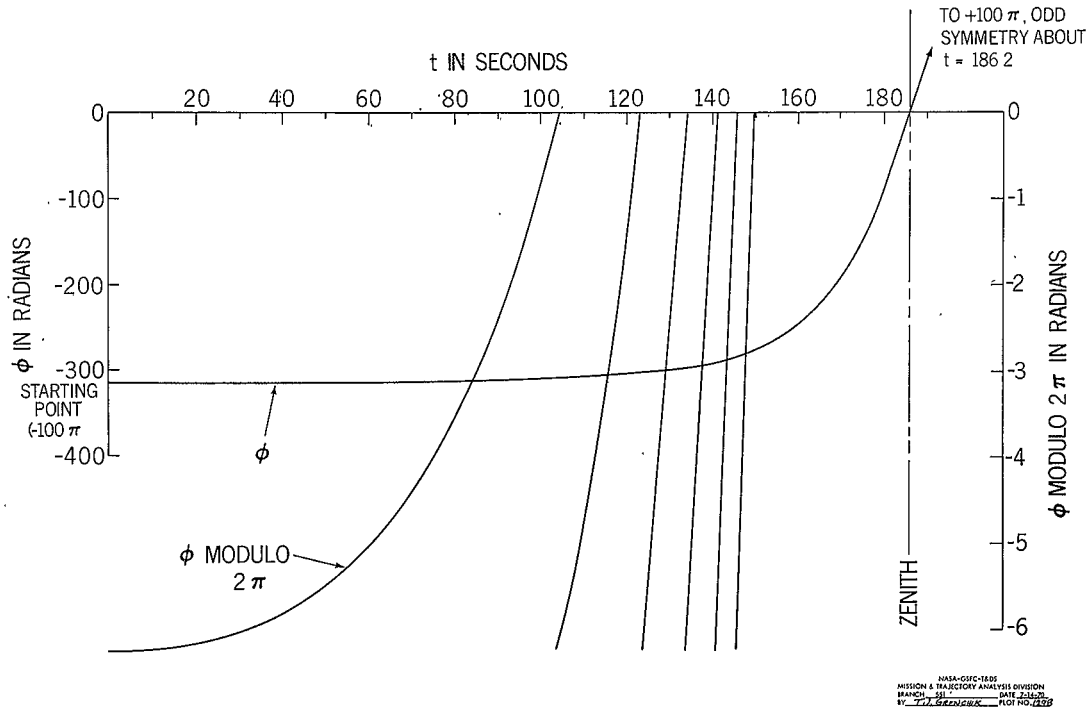

Figure 6. ϕ and ϕ Modulo 2π, h_s = 100 Statute Miles

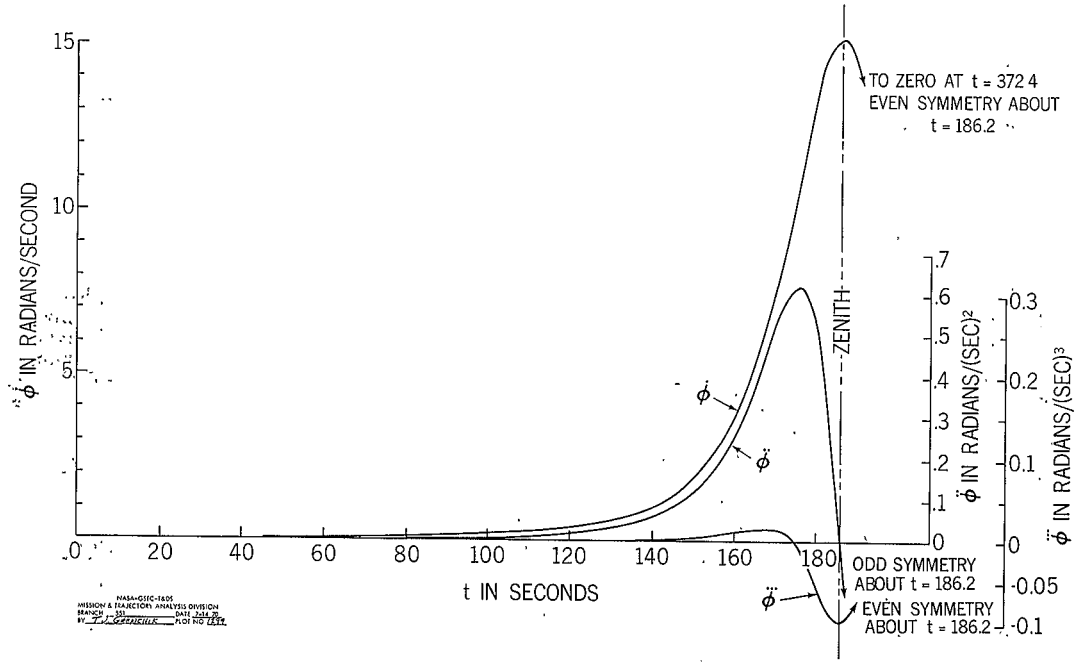

Figure 7. $\dot{\phi}$, $\ddot{\phi}$, and $\dddot{\phi}$; h_s = 100 Statute Miles

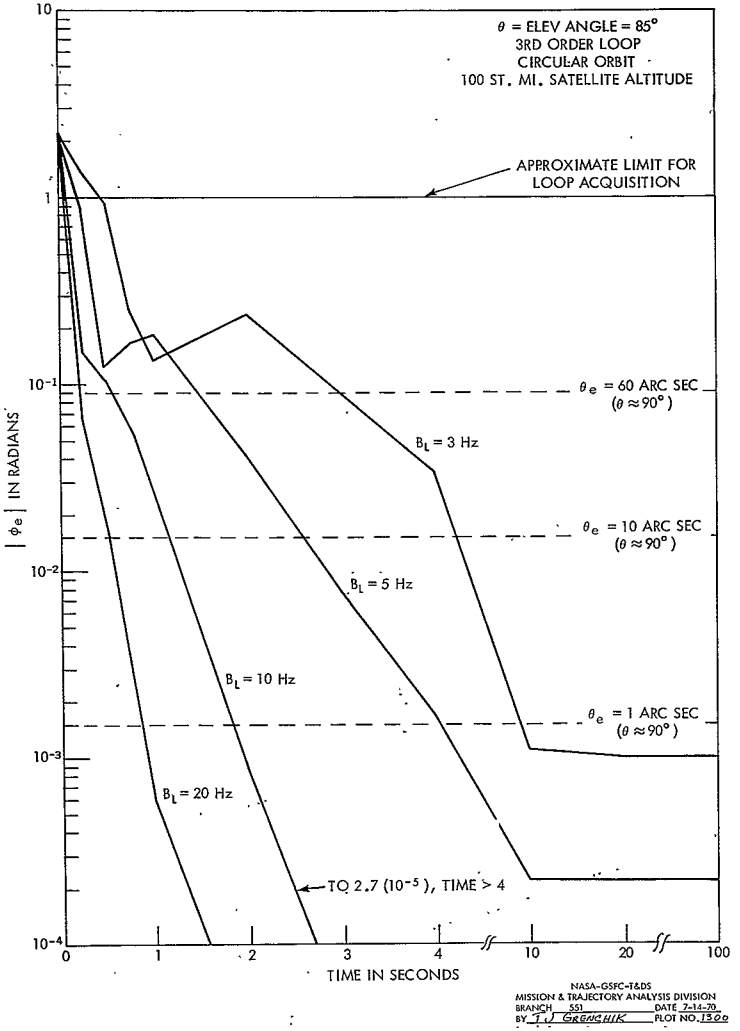

Figure 8. Absolute Value of Phase Error at Loop Output for Time After Acquisition Attempted ($\theta = 85°$; t = 184.4 Sec into Pass)

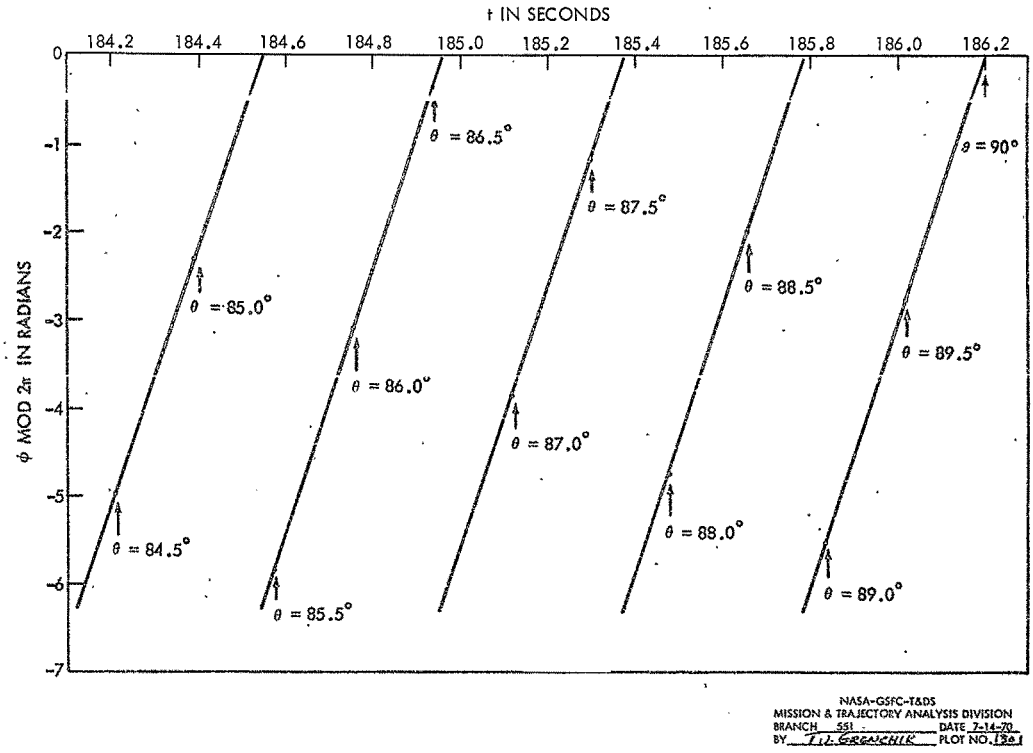

Figure 9. ϕ Mod 2π, h_s = 100 Statute Miles, $84° < \theta < 90°$

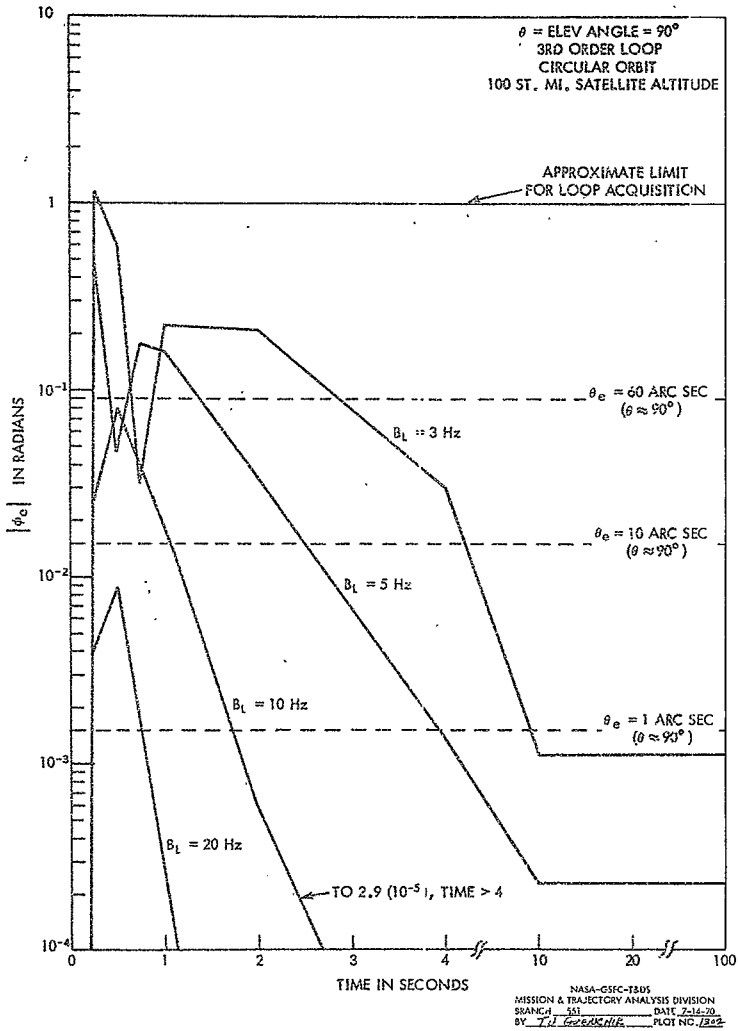

Figure 10. Absolute Value of Phase Error at Loop Output for Time After Acquisition Attempted ($\theta = 90°$, t :. 186.2 Sec into Pass)

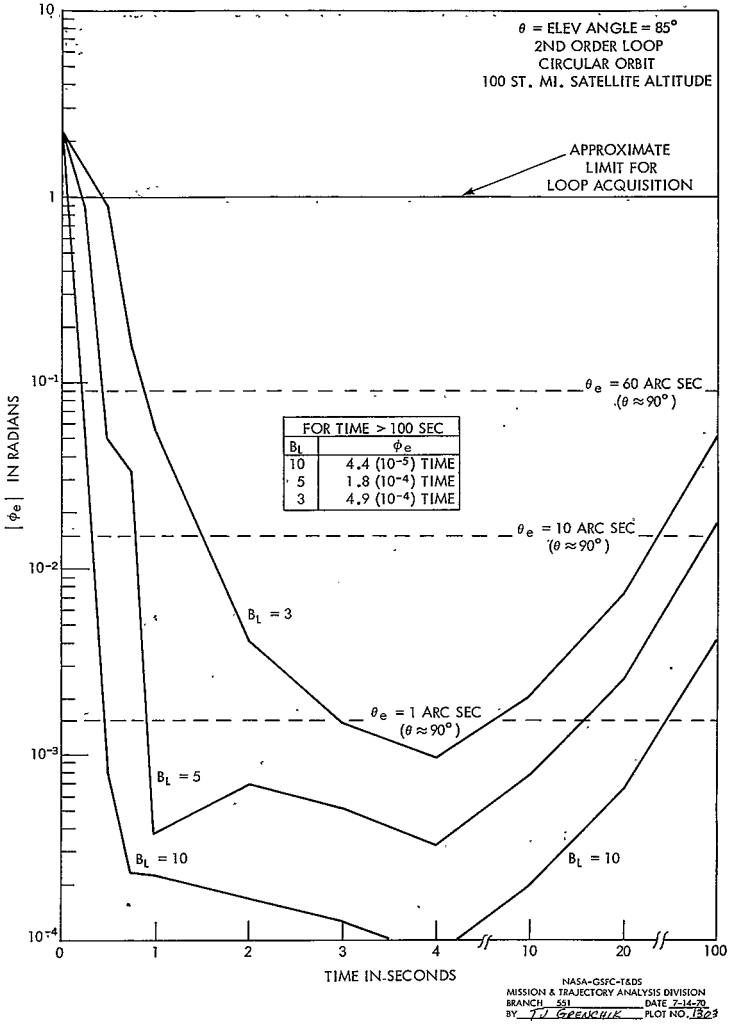

Figure 11. Absolute Value of Phase Error at Loop Output for Time After Acquisition Attempted ($\theta = 85°$, $t = 184.4$ Sec into Pass)

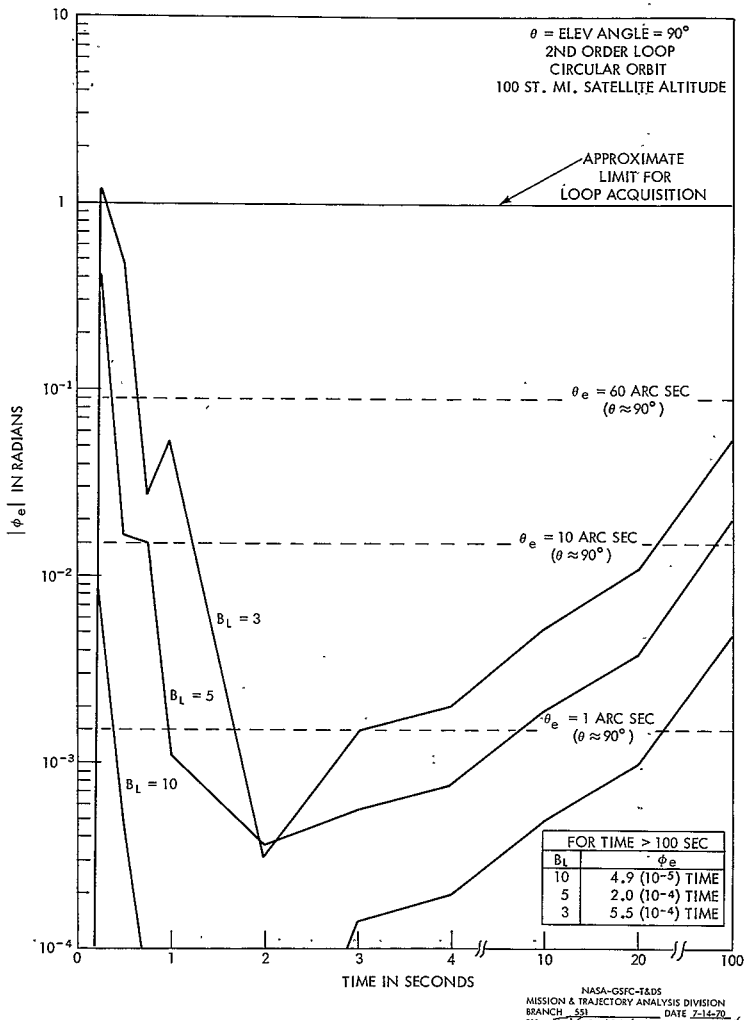

Figure 12. Absolute Value of Phase Error at Loop Output for Time After Acquisition Attempted ($\theta = 90°$, t = 186.2 Sec into Pass)

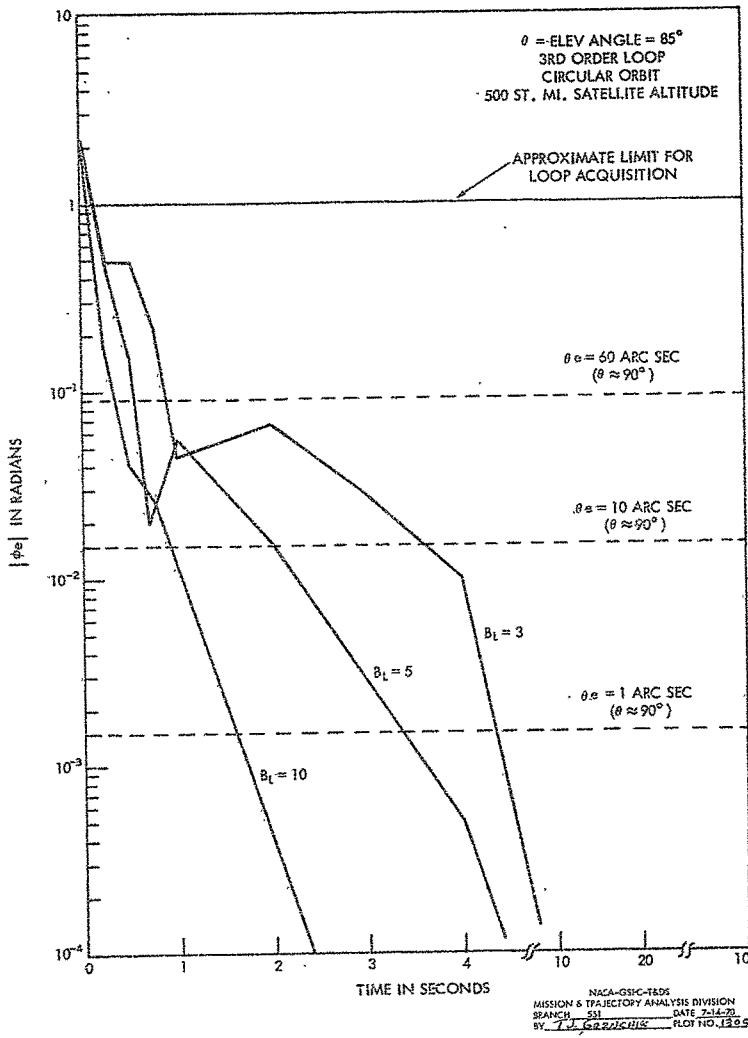

Figure 13. Absolute Value of Phase Error at Loop Output for Time After Acquisition Attempted (θ = 85°, t_i = 451.3 Sec into Pass)

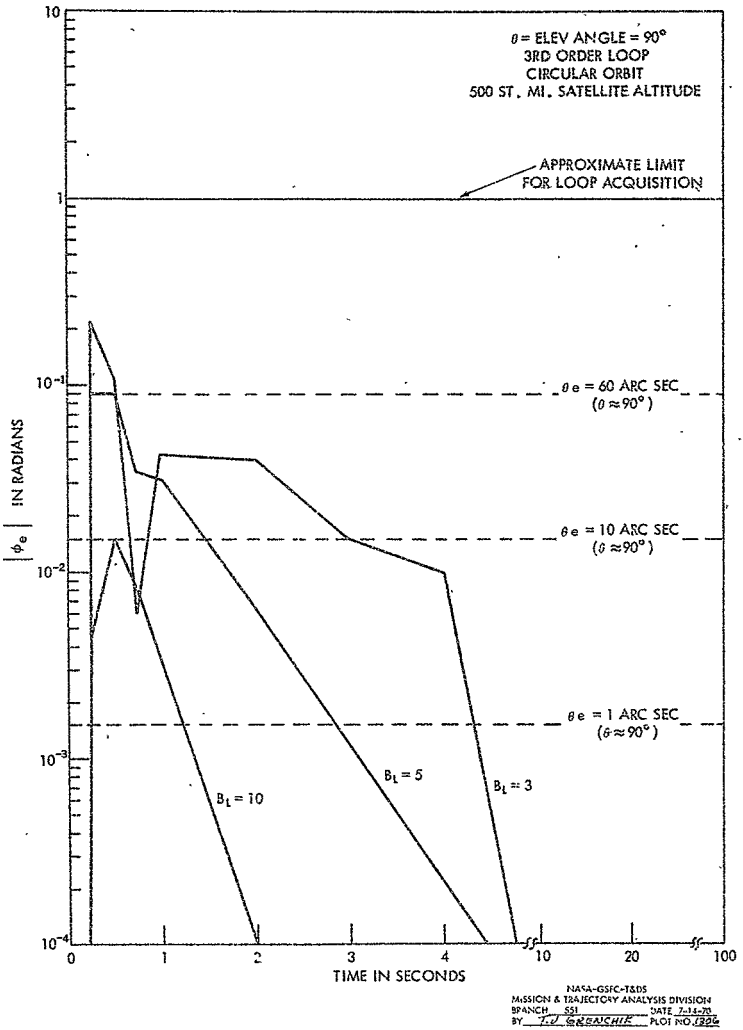

Figure 14. Absolute Value of Phase Error at Loop Output for Time After Acquisition Attempted ($\theta = 90°$, t = 460.8 Sec into Pass)

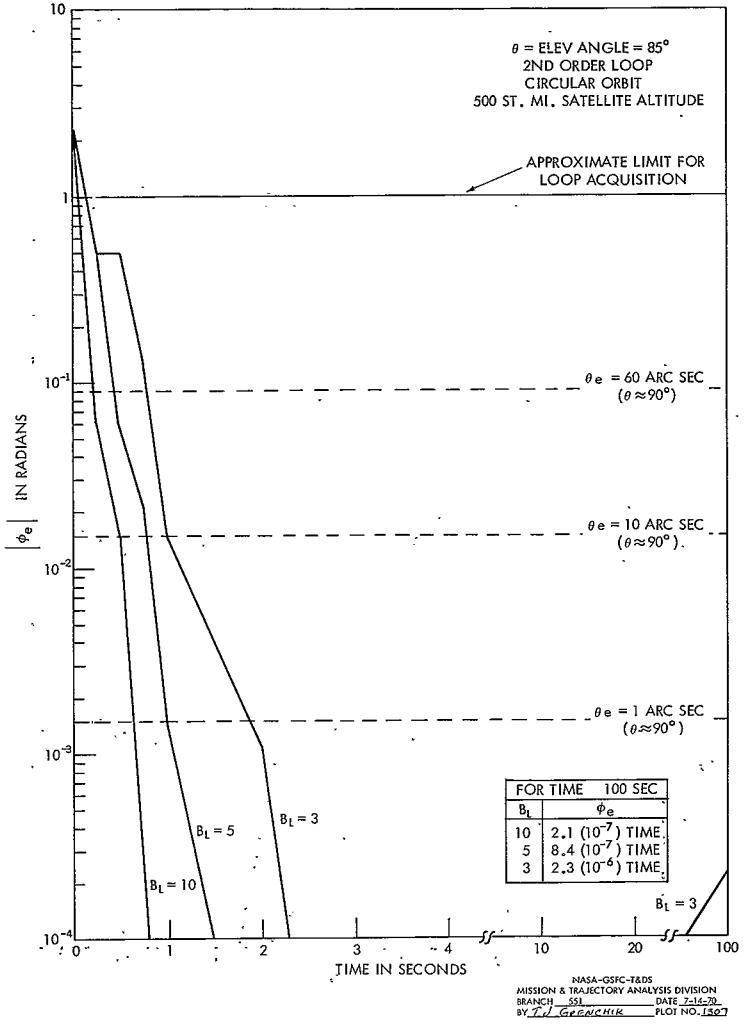

Figure 15. Absolute Value of Phase Error at Loop Output for Time After Acquisition Attempted ($\theta = 85°$, t = 451.3 Sec into Pass)

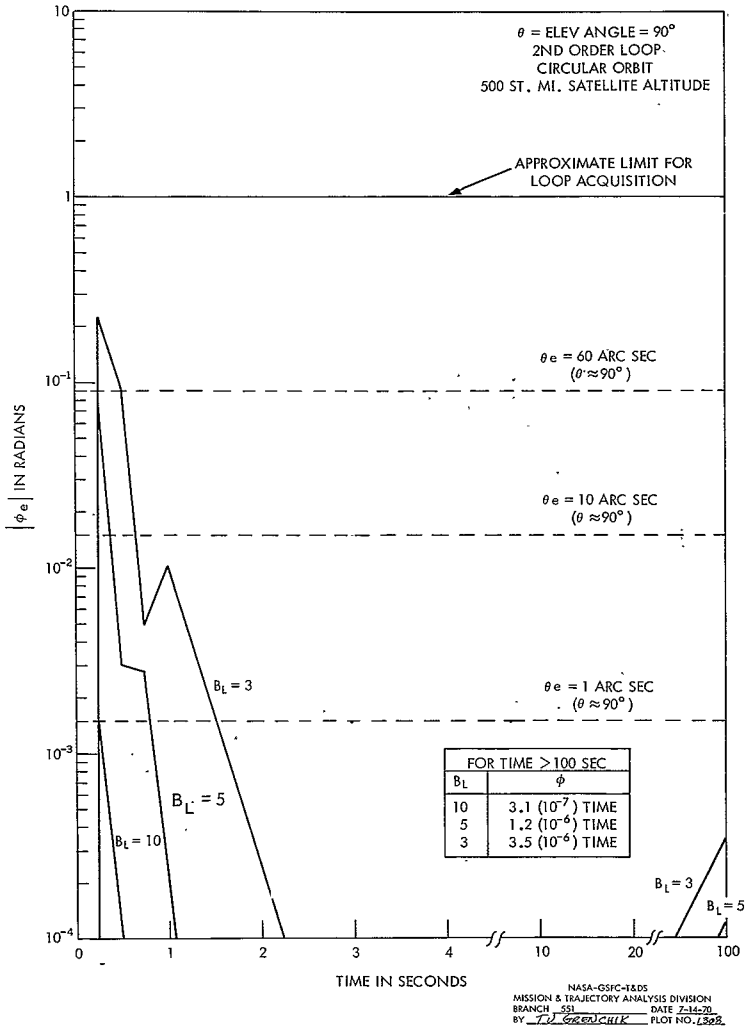

Figure 16. Absolute Value of Phase Error at Loop Output for Time After Acquisition Attempted ($\theta = 90°$, t = 460.8 Sec into Pass)

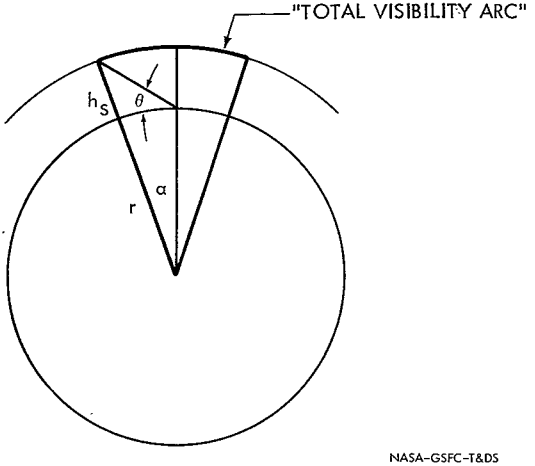

NASA-GSFC-T&DS
MISSION & TRAJECTORY ANALYSIS DIVISION
BRANCH 551 DATE 7-14-70
BY C.W. MURRAY PLOT NO. 1309

Figure 17. "Total Visibility Arc" For An Overhead Pass
Note: Not Drawn to Scale

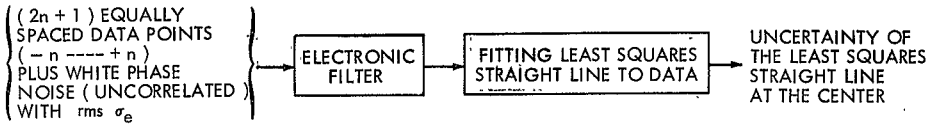

NASA-GSFC-T&DS
MISSION & TRAJECTORY ANALYSIS DIVISION
BRANCH 551 DATE 7-14-70
BY C W MURRAY PLOT NO: 1310

Figure 18. Flow of Information

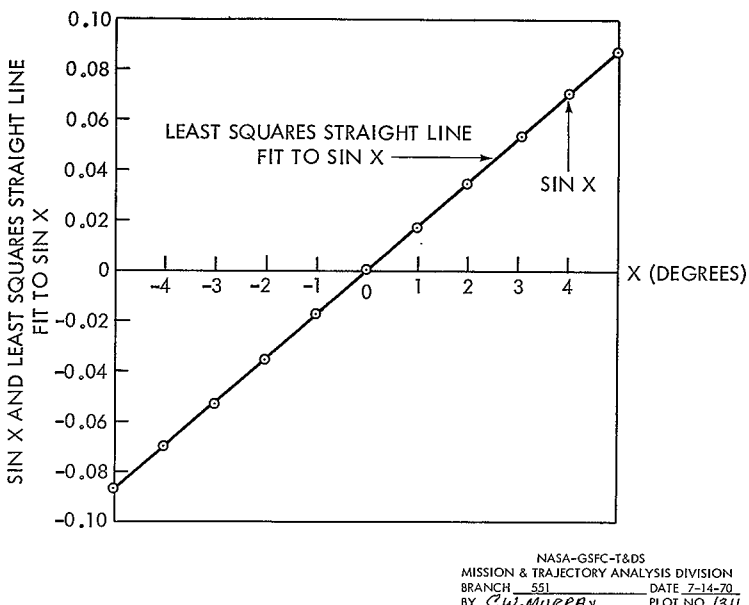

Figure 19. Comparison of Least Squares Straight Line Fit to Sin X with Sin X Evaluated At Several Points ($X = 90 - \theta$ = Interferometer Angle)

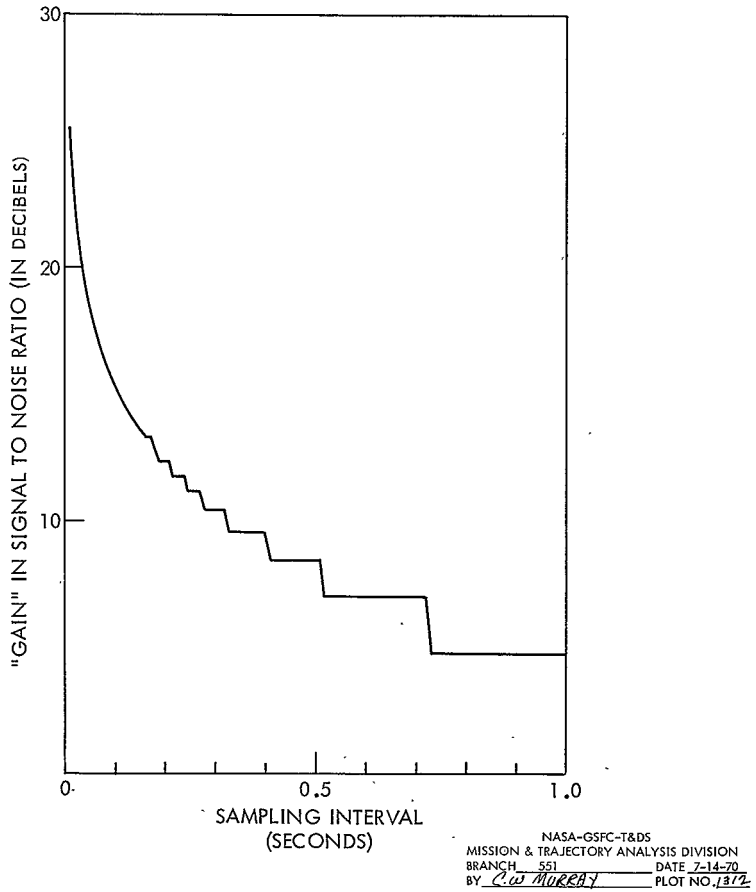

Figure 20. "Gain" Due to Least Squares Smoothing. Uncorrelated Noise
100 Statute Mile Orbit (T = 3.6 Seconds)

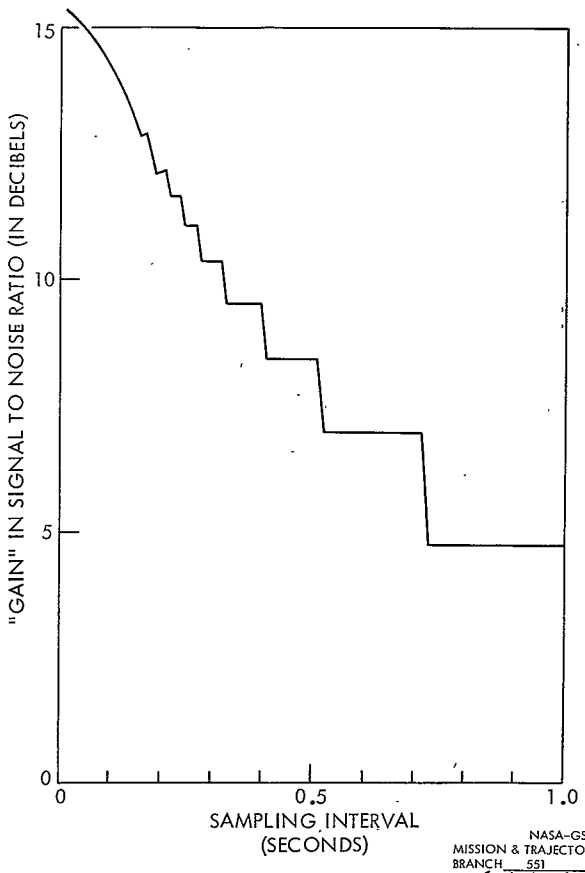

Figure 21. "Gain" Due to Least Squares Smoothing. Single Pole Filter, 3Hz Bandwidth 100 Statute Mile Orbit (T = 3.6 Seconds)

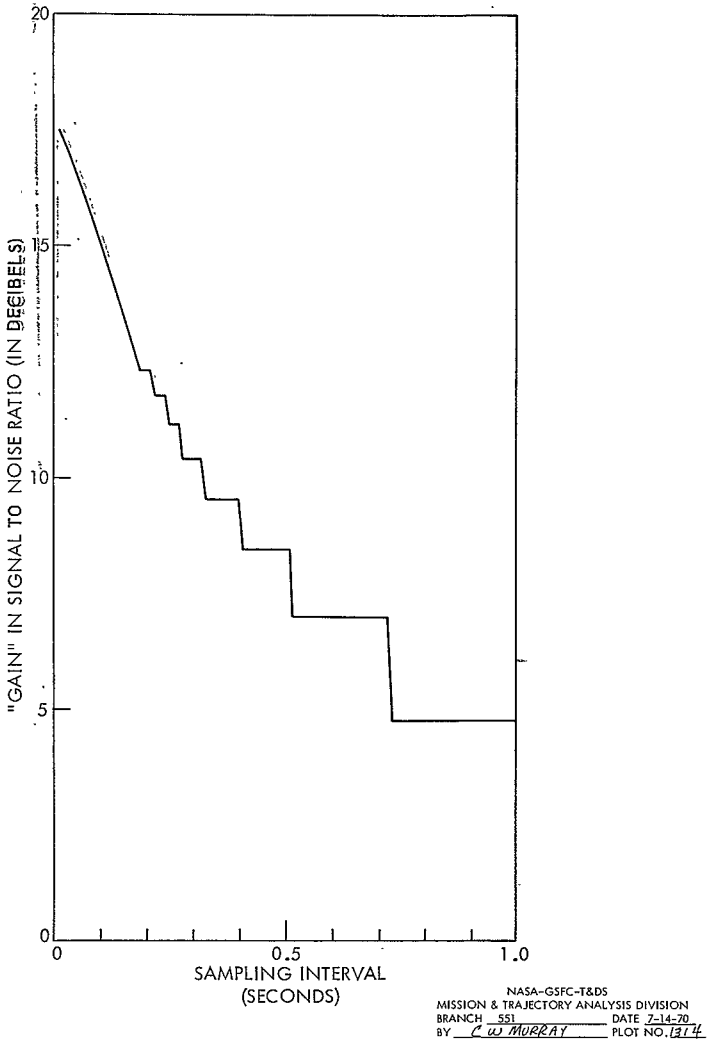

Figure 22. "Gain" Due to Least Squares Smoothing. Single Pole Filter 5Hz Bandwidth 100 Statute Mile Orbit (T = 3.6 Seconds)

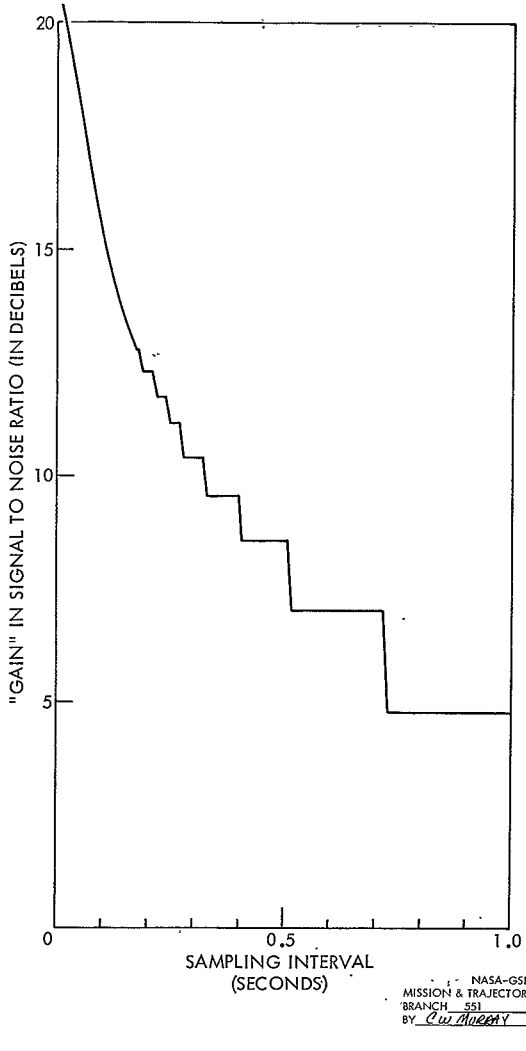

Figure 23. "Gain" Due to Least Squares Smoothing. Single Pole Filter, 10Hz Bandwidth 100 Statute Mile Orbit (T = 3.6 Seconds)

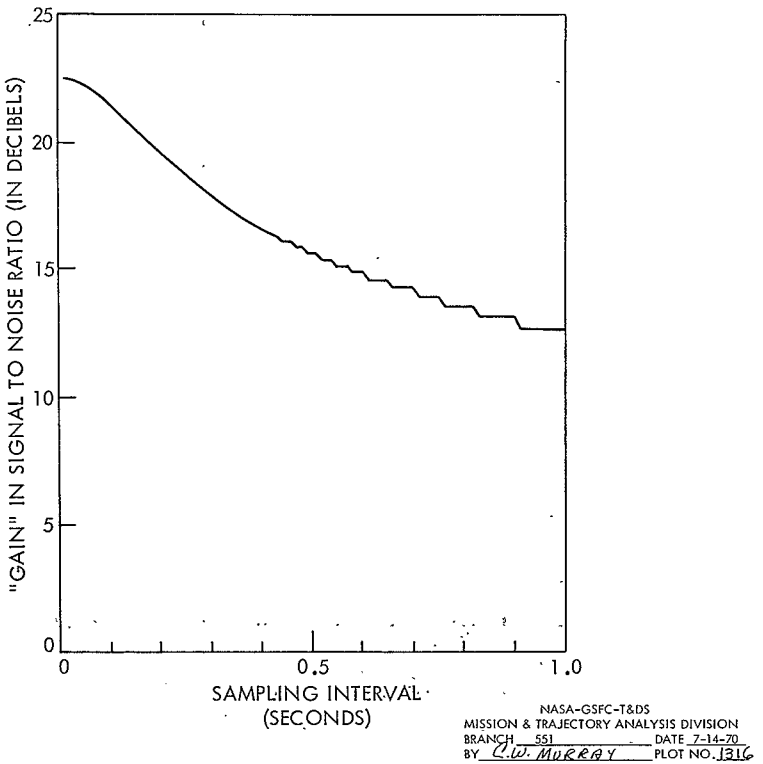

Figure 24. "Gain" Due to Least Squares Smoothing. Single Pole Filter 3 Hz Bandwidth 500 Statute Mile Orbit (T= 18.9 Seconds)

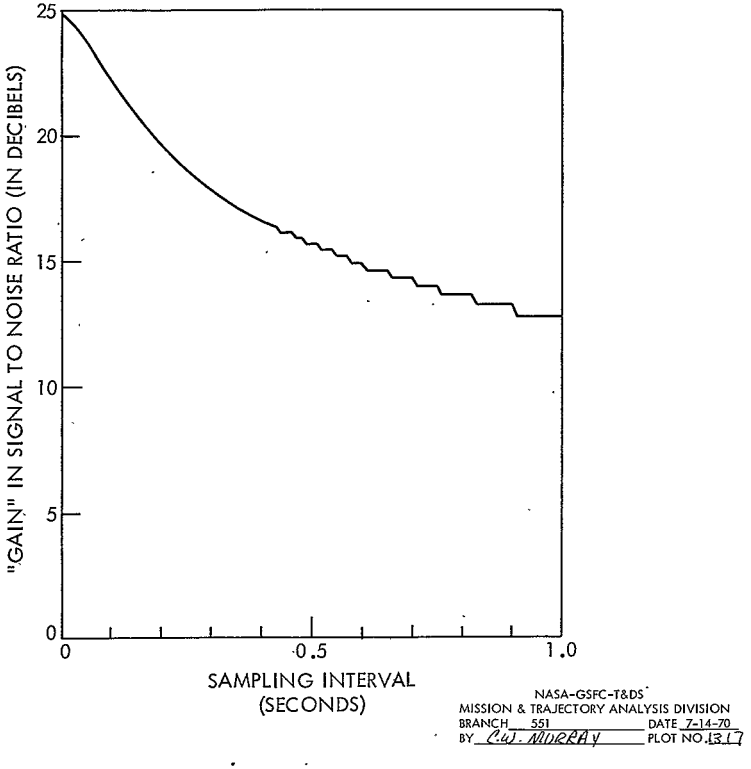

Figure 25. "Gain" Due to Least Squares Smoothing. Single Pole Filter 5Hz Bandwidth 500 Statute Mile Orbit (T= 18.9 Seconds)

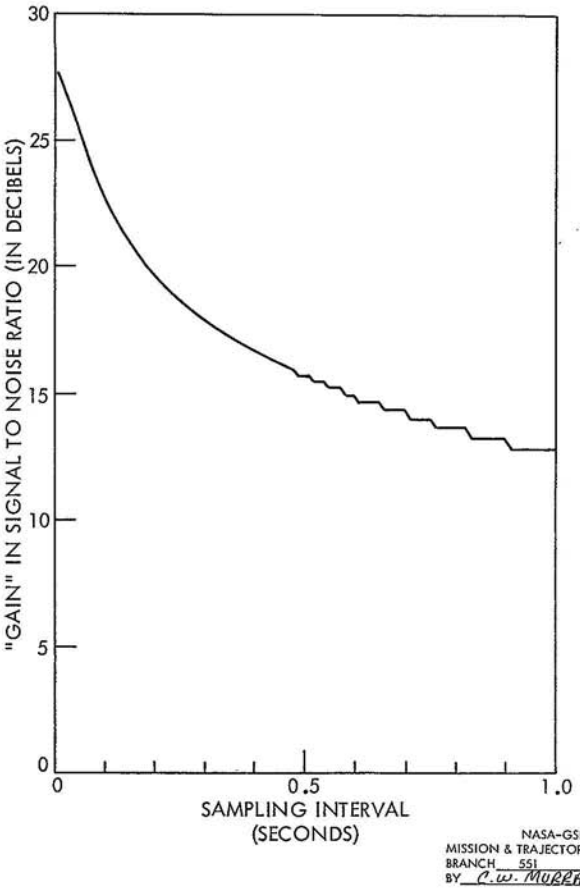

Figure 26. "Gain" Due to Least Squares Smoothing. Single Pole Filter 10 Hz Bandwidth 500 Statute Mile Orbit (T = 18.9 Seconds)

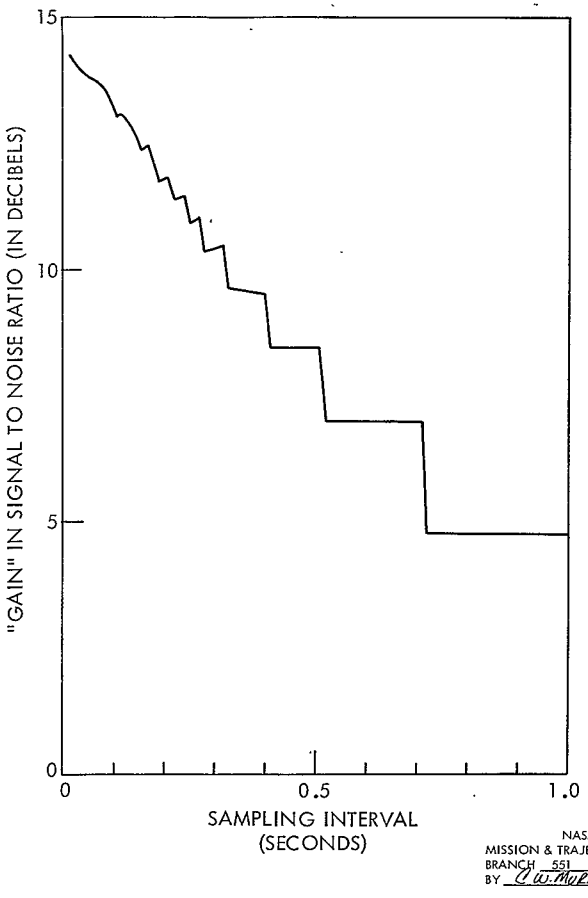

Figure 27. "Gain" Due to Least Squares Smoothing Double Pole Filter 3 Hz Bandwidth
100 Statute Mile Orbit (T = 3.6 Seconds)

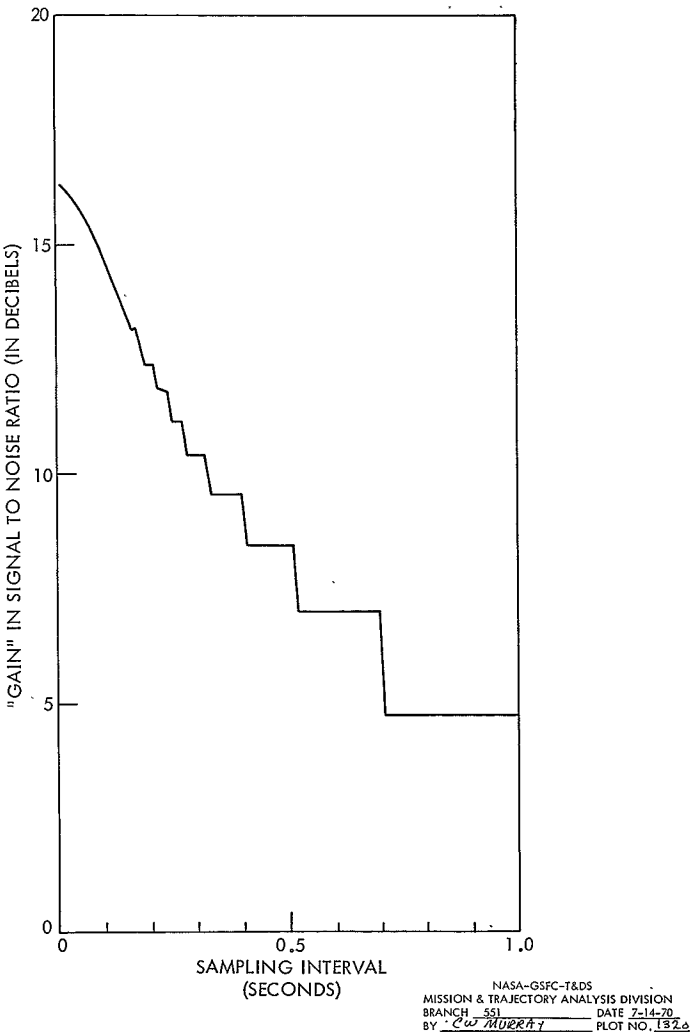

Figure 28. "Gain" Due to Least Squares Smoothing. Double Pole Filter 5 Hz Bandwidth 100 Statute Mile Orbit (T = 3.6 Seconds)

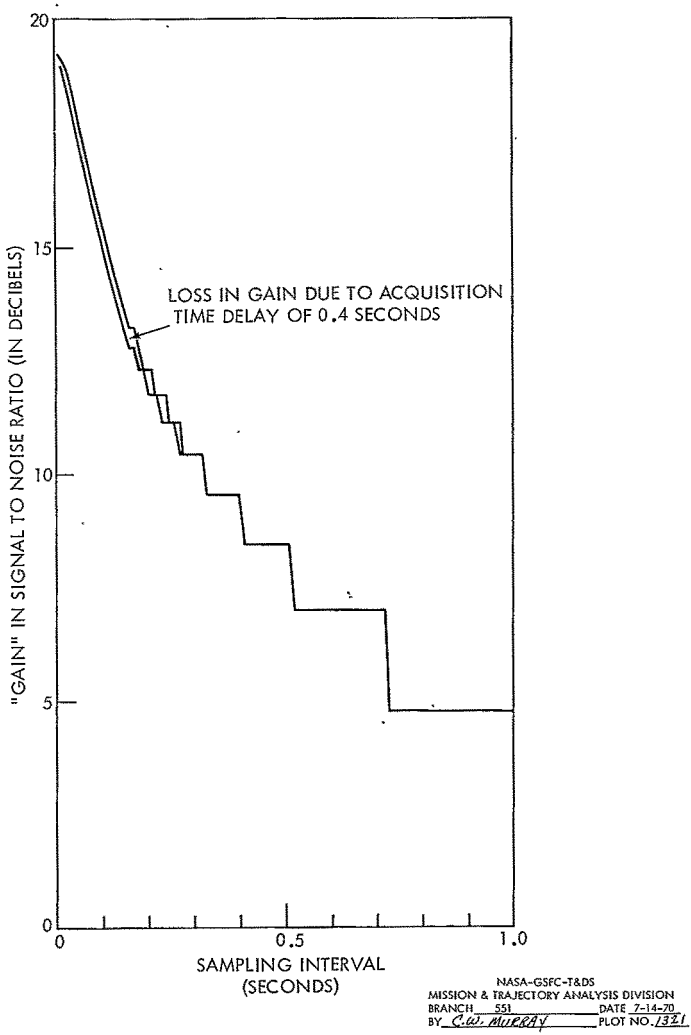

Figure 29. "Gain" Due to Least Squares Smoothing. Double Pole Filter 10 Hz Bandwidth 100 Statute Mile Orbit (T = 3.6 Seconds)

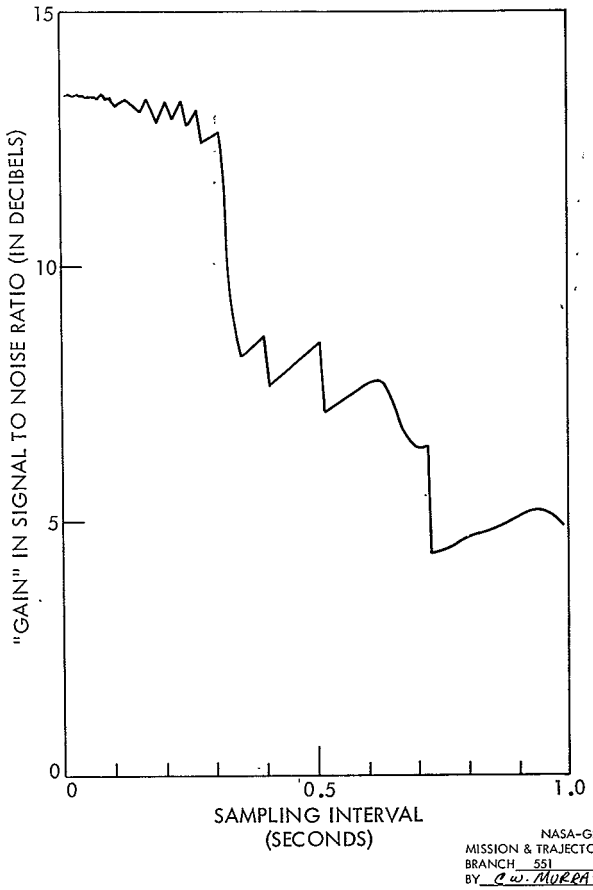

Figure 30. "Gain" Due to Least Squares Smoothing. Ideal Filter 3Hz Bandwidth
100 Statute Mile Orbit (T = 3.6 Seconds)

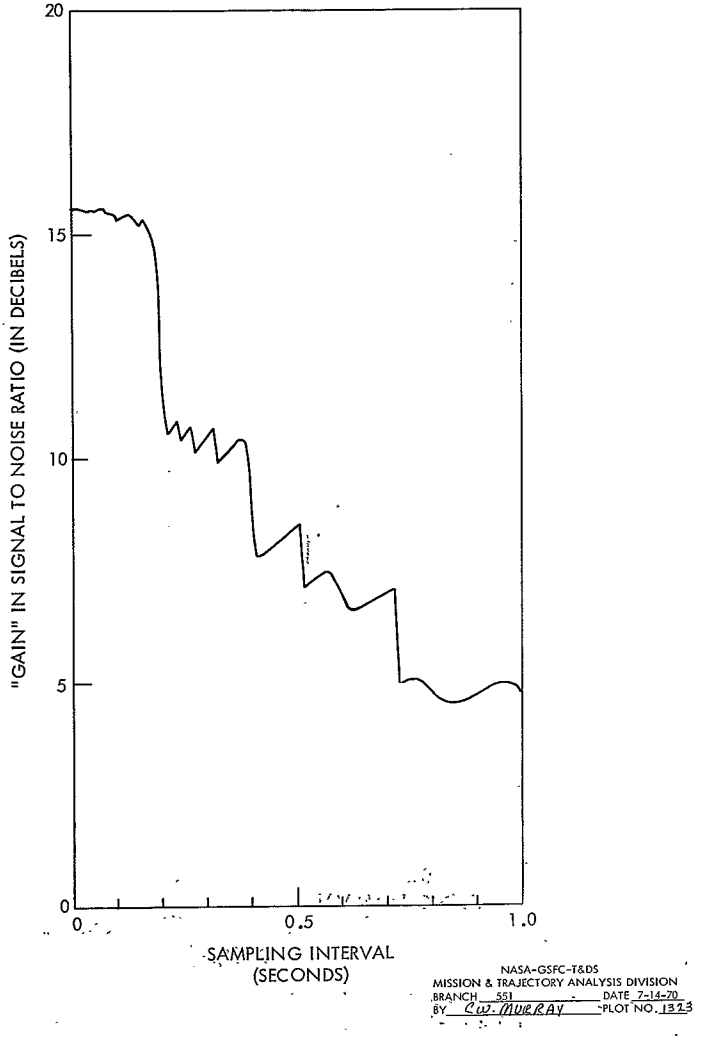

Figure 31. "Gain" Due to Least Squares Smoothing. Ideal Filter 5Hz Bandwidth 100 Statute Mile Orbit (T = 3.6 Seconds)

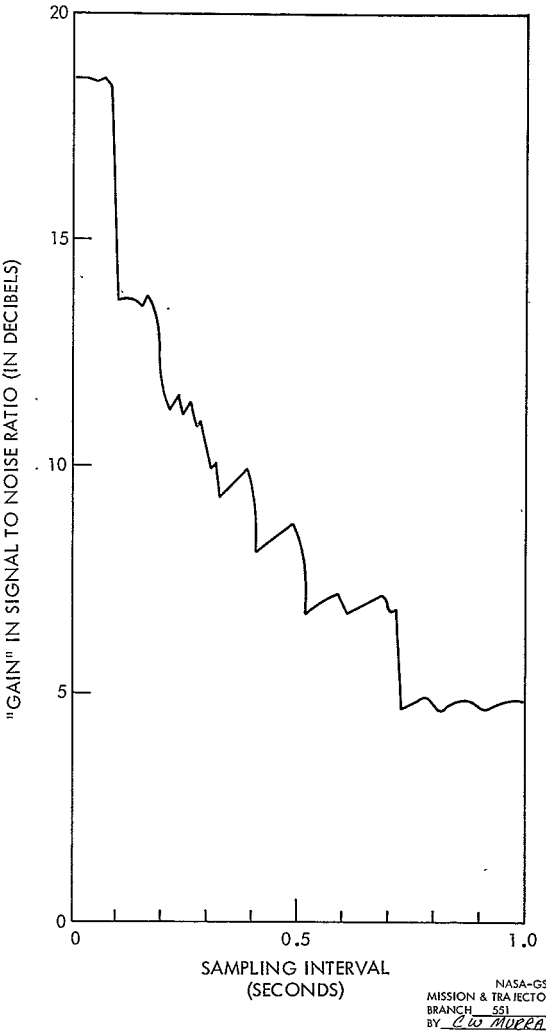

Figure 32. "Gain" Due to Least Squares Smoothing. Ideal Filter 10 Hz Bandwidth 100 Statute Mile Orbit (T = 3.6 Seconds)

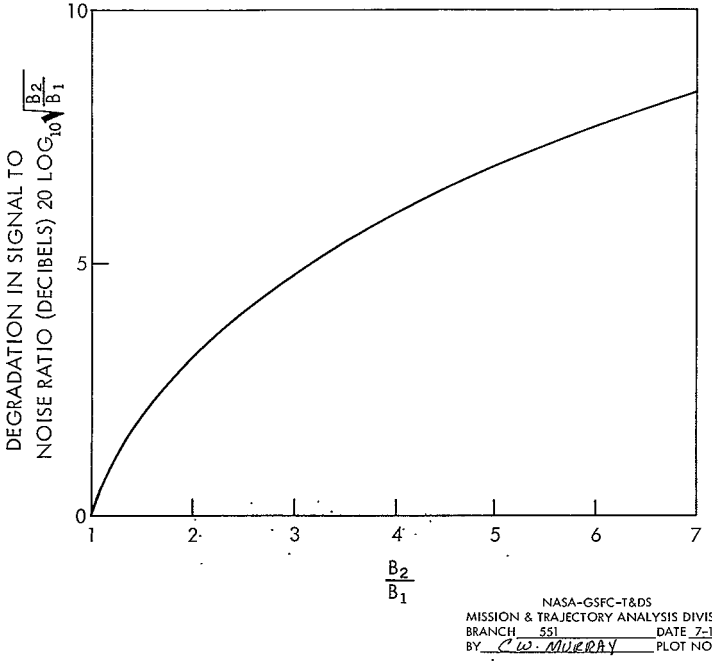

Figure 33. Noise Degradation in DB Due to Increased Bandwidth